BRNO UNIVERSITY OF TECHNOLOGY
VYSOKÉ UČENÍ TECHNICKÉ V BRNĚ

FACULTY OF MECHANICAL ENGINEERING
FAKULTA STROJNÍHO INŽENÝRSTVÍ

INSTITUTE OF MATERIALS SCIENCE AND ENGINEERING
ÚSTAV MATERIÁLOVÝCH VĚD A INŽENÝRSTVÍ

MEASUREMENT OF SURFACE TENSION FOR SURFACE CHARACTERIZATION OF ADVANCED CERAMIC MATERIALS

MĚŘENÍ POVRCHOVÉHO NAPĚTÍ PRO CHARAKTERIZACI POVRCHŮ POKROČILÝCH KERAMICKÝCH MATERIÁLŮ

MASTER'S THESIS
DIPLOMOVÁ PRÁCE

AUTHOR — **Bc. Liliana Mišáková**
AUTOR PRÁCE

SUPERVISOR — **doc. Ing. David Salamon, Ph.D.**
VEDOUCÍ PRÁCE

BRNO 2020

BRNO UNIVERSITY OF TECHNOLOGY
FACULTY OF MECHANICAL ENGINEERING

Assignment Master's Thesis

Institut:	Institute of Materials Science and Engineering
Student:	**Bc. Liliana Mišáková**
Degree programm:	Applied Sciences in Engineering
Branch:	Materials Engineering
Supervisor:	**doc. Ing. David Salamon, Ph.D.**
Academic year:	2020/21

As provided for by the Act No. 111/98 Coll. on higher education institutions and the BUT Study and Examination Regulations, the director of the Institute hereby assigns the following topic of Master's Thesis:

Measurement of surface tension for surface characterization of advanced ceramic materials

Brief Description:

The surface of the ceramic material is exposed to various environmental influences, which greatly changes the surface properties of these materials. Layer of oxides, hydroxides or carbonates are present on the surface and have the hydrophilic character. However, recent research by advanced analytical tools such as XPS indicates adsorption of various organic molecules on the surface of ceramic material. These organic molecules significantly changes the surface tension. Aim of this diploma thesis is to characterize changes of surface tension caused by adsorption of organic molecules on the ceramics. Described behavior will have high implication in the field of polymer–ceramic composites.

Master's Thesis goals:

1. Description of state of art and methods suitable for characterization of organic substances on the surface of ceramic materials.
2. Experimentally evaluate absorption of organic molecules on ceramic surfaces by the surface tension measurements.

Recommended bibliography:

KUMAR, G. and K. N. PRABHU. Review of non-reactive and reactive wetting of liquids on surfaces. Advances in Colloid and Interface Science [online]. 2007, 133(2), 61-89 [cit. 2018-11-09]. DOI: 10.1016/j.cis.2007.04.009. ISSN 00018686. http://linkinghub.elsevier.com/retrieve/pii/S0001868607000747

LANDOULSI, J., M. J. GENET, S. FLEITH, Y. TOURÉ, I. LIASCUKIENE, Ch. MÉTHIVIER and P. G. ROUXHET. Organic adlayer on inorganic materials: XPS analysis selectivity to cope with adventitious contamination. Applied Surface Science [online]. 2016, 383, 71-83 [cit. 2018-11-09]. DOI: 10.1016/j.apsusc.2016.04.147. ISSN 01694332. https://linkinghub.elsevier.com/retrieve/pii/S0169433216309357

Deadline for submission Master's Thesis is given by the Schedule of the Academic year 2020/21

In Brno,

L. S.

prof. Ing. Ivo Dlouhý, CSc.
Director of the Institute

doc. Ing. Jaroslav Katolický, Ph.D.
FME dean

ABSTRACT

The presented thesis theoretically describes methods applied for the characterization of organic substances presented on the surfaces of advanced ceramic materials.
Measurement of contact angles experimentally verifies the changes on surfaces of advanced ceramics. These changes are caused by the contamination of the surface. Adsorption of organic compounds on inorganic surfaces is rather unfavorable, therefore obtained results may provide useful information about the mechanisms of removal of the contaminants from surface.

In the experimental part, water contact angle measurements were used to monitor and describe the changes of surface characteristics of ceramic oxides ZnO, TiO_2, hydroxyapatite, Al_2O_3 and ZrO_2. WCAs for untreated surfaces along with the WCA values for thermally or chemically treated surfaces of studied materials were assessed and compared in order to describe changes in surface energy, hydrophilicity and adhesivity caused by adsorbed organic adlayer. The decrease of contact angle values was achieved by cleaning of the surface with subsequent deprivation of adsorbed molecules.

KEY WORDS

Oxide ceramics, surface energy, contact angle measurement, adsorption of organic compounds, contact angle, sessile-drop method

ABSTRAKT

Povrchy inorganických materiálov, zvlášť kovov alebo kovových oxidov, ktoré sú často charakteristické vysokou povrchovou energiou, sú zvyčajne kontaminované adsorbovanými organickými molekulami. Tieto molekuly majú na povrchy zväčša nepriaznivý vplyv, do značnej miery napríklad ovplyvňujú funkcionalitu a výkonnosť polovodičov a znemožňujú, prípadne sťažujú prevedenie povrchových úprav na povrchoch kovov aj keramík. Taktiež majú nepriaznivý vplyv na priľnavosť.

Adsorbované častice spôsobujú znižovanie hydrofilicity povrchu. Hydrofilicita, adhezivita a zmáčavosť povrchu sa veľmi dobre posudzujú prostredníctvom merania kontaktného uhlu. V tejto práci je značná pozornosť venovaná práve meraniu statického kontaktného uhlu. [10]

Samotné meranie kontaktného uhlu je možné vykonať rôznymi spôsobmi, v tejto práci bol však použitý najvhodnejší prístup, a to metódou „sessile-drop“, teda pokladanej alebo depozitovanej kvapky na meraný povrch. K meraniu bol využitý klasický „sessile-drop goniometer“, teda aparatúra, ktorá pozostávala z nastaviteľného stojanu na vzorky, nad ktorým bol umiestnený zdroj svetla, a objektívu fotoaparátu, ktorý bol prepojený s kamerou zabudovaného smartfónu. Meranie prebiehalo tak, že kvapka s objemom 3μL destilovanej superčistej vody bola depozitovaná na povrch substrátu pomocou mikroinjekčnej striekačky. Akonáhle bola kvapka deponovaná, bola vytvorená fotografia, ktorá bola následne spracovaná v programe ImageJ. Pomocou softvéru na vyhodnocovanie kontaktných uhlov boli určené priemerné kontaktné uhly celkom u všetkých vzoriek.

Týmto spôsobom boli charakterizované povrchy všetkých keramických oxidov. Cieľom tejto práce bolo nielen stanoviť kontaktné uhly a porovnať ich hodnoty medzi rôznymi typmi materiálov navzájom, ale hlavne prostredníctvom meraní kontaktných uhlov overiť zmeny na povrchoch, ktoré spôsobuje adsorbovaná vrstva organických molekúl. Všetky typy vzoriek boli po dobu aspoň troch dní vystavené okolitému prostrediu a následne boli uskutočnené primárne (základné) merania. Ďalej boli na rovnakých vzorkách prevedené úpravy tepelného a/lebo chemického charakteru. Po každej takejto úprave boli opäť merané a vyhodnocované hodnoty kontaktných uhlov. Takto vyhodnotené údaje zachycovali zmeny, ku ktorým došlo na povrchoch daných keramických materiálov pri adsorpcii organických molekúl.

Proces tepelnej úpravy (kalcinácia na teplote 800°C, následne pokles na teplotu 600°C, po celkovú dobu 16 hodín) bol aplikovaný na všetkých typoch vzoriek, kde niektoré sa medzi sebou líšili teplotou slinovania. Ihneď po kalcinácii boli vzorky podrobené meraniu kontaktných uhlov, z ktorého jasne vyplynulo, že hydrofilicita a zmáčavosť povrchu sa zvýšila. Tento jav bol pozorovaný na všetkých vzorkách, a na všetkých vzorkách sa hodnoty kontaktného uhlu líšili veľmi významne od hodnoty, ktorá

bola získaná v tzv. primárnom meraní. Všetky detailné hodnoty a vyhodnotené výsledky sú posudzované v časti diskusia.

Ďalšou úpravou povrchu, ktorá bola vykonaná na vybraných vzorkách, bolo čistenie povrchu etanolom. Proces bol opäť realizovaný na všetkých vzorkách. Potom, ako boli zrealizované všetky merania na kalcinovaných vzorkách, boli všetky tieto vzorky ponorené do etanolu na približne 2 hodiny. Po vybratí vzoriek a ich osušení na vzduchu boli uskutočnené ďalšie merania kontaktných uhlov. Výsledky priniesli opäť rozdielne hodnoty v porovnaní s predchádzajúcimi meraniami a sú rozvinuté v časti diskusia.

Okrem zmien, ktoré indikujú kontamináciu povrchu organickými molekulami, preukázali merania kontaktného uhlu aj trend rastu kontaktného uhlu s rastúcou slinovacou teplotou. Táto závislosť je podložená rastom relatívnej hustoty, poklesom porozity a rastom priemernej veľkosti zrna so zvyšovanou slinovacou teplotou.

Popri sledovaných experimentoch boli pozorované aj iné javy, ktoré už neboli predmetom tejto práce, no sú dosť významné na to, aby boli hlbšie preskúmané. Jedna z mnoha zaujímavostí, ktoré boli postrehnuté v priebehu práce, bola napríklad závislosť kontaktného uhlu na veľkosti depozitovanej kvapky. Počas experimentu boli striktne dodržiavané objemy depozitovaných kvapiek, aby sa predišlo situáciám, kde by dochádzalo k častým deformáciám kvapky spôsobenej gravitáciou vzhľadom na jej veľký objem. Zároveň ale nesmie byť veľmi malá, pretože malý objem znemožňuje vyhodnocovanie ako také. Ďalším zaujímavým faktorom, ktorý môže zásadne ovplyvňovať výsledky meraní, je dĺžka expozície vzorku, ktorý podstúpil určité tepelné alebo chemické úpravy, na okolitom vzduchu. S predlžujúcou sa expozíciou dochádza k opätovnému zvyšovaniu kontaktných uhlov, a teda povrchového napätia, čo je spôsobené ďalšou adsorpciou organických molekúl prítomných v ovzduší.

Záver práce hodnotí všetky dosiahnuté výsledky. Posudzuje zmeny pozorované na povrchoch materiálov, ktoré sú spôsobené adsorpciou organických kontaminantov. Vyhodnocuje výsledky a mieru úspešnosti jednotlivých povrchových úprav, ktoré prispeli k čiastočnej eliminácii adsorbovaných organických molekúl na povrchoch jednotlivých keramických materiálov.

KĽÚČOVÉ SLOVÁ

Oxidová keramika, povrchové napätie, meranie kontaktného uhlu, adsorpcia organických zlúčenín, kontaktný uhol, metóda sessile-drop

BIBLIOGRAPHIC CITATION

MIŠÁKOVÁ, Liliana. *Měření povrchového napětí pro charakterizaci povrchů pokročilých keramických materiálů* [online]. Brno, 2020 [cit. 2020-06-25]. Dostupné z: https://www.vutbr.cz/studenti/zav-prace/detail/121634. Diplomová práce. Vysoké učení technické v Brně, Fakulta strojního inženýrství, Ústav materiálových věd a inženýrství. Vedoucí práce David Salamon.

DECLARATION

I hereby declare that this master's thesis *'Measurement of surface tension for surface characterization of advanced ceramic materials'* has been compiled solely on my own following the instructions of my master's thesis supervisor and using of sources listed in Literature section.

Brno, 11th of September 2020 …..……..

Bc. Liliana Mišáková

ACKNOWLEDGEMENTS

I would like to express my gratitude to my supervisor doc. Ing. David Salamon, Ph.D. for his continuous help, guidance, valuable advice and recommendations, proffesional scientific supervision, his patience and attitude throughout the whole 3 years of my master's degree studies. I would also like to thank Ing. Tomáš Spusta, Ph.D. for his initiative help and assistance in laboratories. Furthermore, I would like to thank Maliha Siddiqui for helping me with sample preparation and microstructure evaluation using SEM technology. Last but not least,, my thanks go to CEITEC Institute, Brno University of Technology for allowing me the use of laboratory equipment needed to perform the experimental part of this work.

I am also thankful for the unconditional support of my family members throughout my whole studies.

TABLE OF CONTENTS

1 INTRODUCTION

Ceramic materials are characterized as solid, inorganic compounds of atoms formed by application of heat or both heat and pressure. Type of chemical bonding, density, crystal structure and other factors determine the surface properties of every ceramic material.

Surface properties, such as wettability, surface energy or hydrophilicity, are very important factors in terms of surface modification and treatment. According to these properties, surfaces of given materials are less or more likely to adsorb particles on their surface. Surface characteristics may be assessed by various methods.

Contact angle measurements may seem as a very simple method of surface energy determination. Although, the simplicity may be misleading regarding the reproducibility of measured values. This thesis precisely describes the sessile-drop measurement method and explains the origin of contact angle hysteresis. Contact angle measurements provide useful information about surface characteristics, that are crucial for the assessment of changes on surfaces due to organic compound contamination.

The influence of adsorption of organic contaminants on inorganic surfaces is significant. Moreover, volatile organic compounds present in the atmosphere are very easily adsorbed on the surfaces of inorganic materials, such as oxide ceramics. The adsorption of organic contaminants is not favorable as they change surface characteristics of the substrate. Adsorbed molecules should be removed prior to any intended surface treatment or modification, otherwise the efficiency of such treatment may be influenced. Surface changes caused by organic adlayers are assessed in the experimental part of this thesis.

2 GOALS OF THE WORK

The aims of this master's thesis are:

- Theoretical description of the current state of the art and assessment of convenient methods for the characterization of organic substances on the surface of ceramic materials
- Experimental verification of changes on the surfaces of ceramic materials caused by the adsorption of organic contaminants

3 THEORETICAL PART

This part of work is referring to the general characterization of advanced ceramic materials such as alumina, zirconia, hydroxyapatite and other technical ceramics. In the following section are described some of the physical, chemical and technological properties. Further sections are focused on surface energy, surface characterization by measurements of contact angles, and, lastly, on the adsorption of organic compounds on the inorganic surfaces.

3.1 Ceramic materials

Ceramic material is usually defined as a solid compound of metal, non-metal and metalloid atoms formed by the application of heat or both heat and pressure. Atoms are held in ionic, covalent, metallic or mixed bonds. The large family of ceramic materials comprises polycrystalline and single-crystal inorganic materials, amorphous glasses, and glass-ceramics. [1], [2]

Generally, from the application point of view, one can distinguish traditional and advanced ceramics. The traditional ceramics may include pottery, sanitary ware, tableware, bricks, etc., while the advanced ceramics is usually referred to as technical ceramics.

The classification of advanced ceramic materials can be provided in many ways, one of which is the classification based on their chemical composition-oxides, carbides, nitrides, etc. Another way is to classify them by their major function, such as electronic, optical, magnetic ceramics, or by their microstructure. [2], [3]

It is necessary to add that both the chemical composition and chemical bonding between atoms have a direct impact on the ceramics' properties and its application. In order to understand the variations of properties of materials, it is essential to reveal how the atoms of the solid are bonded. Types of chemical bondings that may be present in ceramic materials are described in the following section.

3.1.1 Chemical bonding in ceramics

According to the strength of the bonding, 2 types of chemical bonds may be distinguished-primary (stronger) bonds and secondary (weaker) bonds. The cohesion of solids is a result of the attractive electrostatic interaction between the nuclei and the electrons, thus between the positive and negative charges, respectively. [1]

3.1.1.1 Primary bonding

Speaking of primary bonds, ionic, covalent and metallic bonds occur among materials. Ceramics are most commonly ionically or covalently bonded, although it is important to

mention that the bonding is neither purely covalent nor purely ionic. Usually, the bonding is a mixture of these two with a predominance of one type over another.

The metallic bond is the primary bond among metals. It is referred to as an electrostatic interaction between the ion cores of atoms and their delocalized valence electrons, thus an interaction between positively charged ions and negatively charged electron gas surrounding the array of cations.

A covalent bond forms by sharing of valence electrons among two or more atoms. The formation of a pure covalent bond is related to the electronegativity of participating atoms. If two combining atoms are those of the same element, thus have the same value of electronegativity, the electrons are shared equally. Although, when it comes to a combination of two different atoms, the values of electronegativities differ as well, therefore the formed bond is not purely covalent, but has a large covalent component. Such a bond can be found in alumina between the atoms of Al and O.

The ionic bond forms when it comes to a complete transfer of valence electrons from one atom to another. The outer energy shell of the donating atom empties, while the one of an accepting atom fulfills. This type of bond results in the formation of a cation-anion pair, where both of them acquire the configuration of an inert gas. It is the attraction between oppositely charged ions which forms the actual bonding. A usual example of ionic bonding is the one of NaCl. However, pure ionic compounds do not exist. Every „ionic" compound has a smaller or greater covalent part. [1-3]

In mostly every material, two or more types of bondings are present. Either it is a mixture of covalent and metallic in case of iron, or it may be a mixture of metallic and ionic, or covalent and ionic bond.
Compounds being a combination of metallic and nonmetallic elements, such as ceramics and semiconductors, are known for having covalent bonding as well as ionic bonding. The more the electronegativity of the elements differs, the greater the ratio of ionic bonding is, following equation (1) below:

$$Fraction\ of\ ionic\ character = 1 - \exp[-0{,}25 \cdot (X_M - X_X)^2]\ (-), \quad (1)$$

where: X_M is the electronegativity of cation (-)
X_X is the electronegativity of anion (-)

Even though no compound has purely ionic nor purely covalent bonding, ceramics with higher ratio of covalent bonding are referred to as „covalent" ceramics, whilst ceramics that are predominantly ionically bonded are referred to as „ionic" ceramics. Many oxide ceramics, with Al_2O_3, TiO_2, and ZrO_2 counting, are characterized by the predominance of ionic bonding since the electronegativities of elements differ by a major margin.
The directionality of bondings is also very important when it comes to the properties of

materials. It affects the way the material responds to deformation and thus influence its mechanical properties. [2], [4]

3.1.1.2 Secondary bonding

Secondary bonds are weaker compared to the primary bonds, although they are important in determining properties or crystal structure of a material.

Van der Waals interaction (London interaction) is an electrostatic attractive force between electroneutral atoms or molecules which are separated by a smaller distance. The existence of such a force is justified by the fluctuating charge distribution in an atom. Given that this bonding is of a smaller strength than primary bondings, it is only important when it is not defeated by stronger forces.
The energy of crystal containing secondary van der Waals bonding is expressed by empirically obtained potentials such as Morse potential or Lennard-Jones potential, as follows:

$$E = -\frac{A_{LJ}}{r^6} + \frac{B_{LJ}}{r^{12}} \quad (J), \tag{2}$$

where: E is the energy of crystal (J),
r is the distance (m),
A_{LJ}, B_{LJ} are constants of the Lennard-Jones potential (Jm^6), (Jm^{12}), respectively.

The equation implies that A_{LJ} represents a repulsive term and B_{LJ} the attractive one. Nonetheless, both terms decrease rapidly with increasing interatomic or intermolecular distance r. The rate of decrease is much greater than the one of Coulomb electrostatic forces, therefore secondary bondings are of much shorter range than primary bonds. [4]

This kind of bond is important in layered structures, for example, graphite structure. There is a strong covalent bonding within the layer, but a weak van der Waals bonding between the layers. As a consequence, these materials show highly anisotropic behavior.

Van der Waals interaction's importance highly exceeds the microscopic scale. Not only this interaction influences the energy of a crystal, but it also has an impact on other material properties such as wetting. The interaction energy between different macroscopic geometries is given by the Hamaker constant, stated below:

$$\mathcal{A} = \pi^2 A_{LJ} \rho_1 \rho_2 \quad (J), \tag{3}$$

where: $\mathcal{A}$ is Hamaker constant (J),
A_{LJ} is the repulsive term of Lennard-Jones potential (Jm^6),
ρ_1, ρ_2 is a number of atoms per unit volume in two solids (m^{-3}).

Values of Hamaker constant of some oxide ceramics are given in Table 1 below:

Tab. 1: Hamaker constants

Material	$\mathcal{A}$ (zJ)
TiO_2	*430*
ZrO_2	*270*
Al_2O_3	*140*
Fe_3O_4	*210*

Knowledge of these values is critical for the evaluation of the strength of van der Waals forces. Those are obtained by differentiation of interaction energies of each macroscopic geometry.

Van der Waals interaction is not a single type of weak secondary interactions between atoms or molecules. Hydrogen bonds are even stronger, yet they are not considered strong enough to be part of the primary bonds' family. The bond forms when an atom of hydrogen, already covalently bonded, joins another more electronegative atom. The molecule of water is a common example. Again, given that it is a weaker bond, it causes anisotropic behavior of materials with layered structures. [4]

3.1.2 Physical properties of ceramic materials

Out of many physical properties, density and porosity are discussed in this chapter for being the most important ones for this thesis´ purpose.

3.1.2.1 Density

Density is defined as a ratio of mass per unit volume of a material. Its value depends on the atomic weight of specific elements, their diameter and stacking in the cell, as well as on the porosity in the microstructure. The term "density" may relate either to the crystallographic density, theoretical density, bulk density, or specific gravity.

a) Crystallographic density is referred to as the ideal density of a crystal. It is determined from the chemical composition of the crystal, the tightness of atomic stacking and the interatomic distances between specific atoms.
Its value is obtained by dividing the mass of a unit cell by its volume, as following:

$$\rho = \frac{m_{unitcell}}{V_{unitcell}} \ (g \cdot cm^{-3}), \tag{4}$$

where: ρ is the crystallographic density ($g \cdot cm^{-3}$),
$m_{unitcell}$ is the weight of the unit cell (g),
$V_{unitcell}$ is the volume of the unit cell (cm^3).

Assuming from the equation 3.1, the crystallographic density is expected to gain greater values with increasing atomic weight. Another parameter influencing the crystallographic density is the atomic stacking in the structure – the interatomic spacing that affects the volume of the unit cell. The greater the distance between ions or atoms in the crystal is, the lower is the value of density. Close-packed structures, such as ZrO_2, are characterized by bigger crystallographic density compared to the non-close-packed structures. A more illustrating example could be the one of diamond and graphite. The diamond structure comprises strong covalent bondings between the atoms of carbon and thus the length of the bond is shorter. On the other hand, the graphitic structure consists not only of covalent bonds between the carbon atoms but also of secondary van der Waals interactions between the layers, which are considerably weaker than primary bonds. Therefore, the length of the bond is shorter and the volume of the cell is thus greater. As a consequence, graphite shows a smaller value of crystallographic density than diamond. A table of crystallographic densities of ceramics studied in this thesis below: [5], [6], [37]

Tab. 2: Crystallographic densities of selected ceramic materials

Material	*Crystallographic density [g·cm^{-3}]*
TiO_2	*3.76*
Al_2O_3	*3.87*
ZrO_2	*5.80*
Hydroxyapatite	*3.08*

b) Bulk density gives out a more adequate value than the crystallographic density. Usually, the material consists of more than one crystalline phase, non-crystalline phase, and also contains some porosity, which is ignored by the calculation of crystallographic density. Hence, there is a slight difference in the bulk density formula:

$$B = \frac{m}{V_{bulk}} = \frac{m}{V_S + V_P} \ \ (g \cdot cm^{-3}), \tag{5}$$

where: m is the mass of the unit cell (g)

V_{bulk} is the volume of the crystalline phases and the porosity (cm^{-3})

V_S is the volume of the solid phase (g·cm^{-3})

V_P is the volume of pores (g·cm^{-3}).

Bulk density is calculated using the Archimedes principle. The volume is determined from the difference of weights of the solid in the air and in the water. Before the start of the measurement, it is critical to assume whether the solids show surface-connected porosity or not. If so, they cannot be immersed into the water directly, but they need to be coated with an impervious material, such as

wax. [5]
There are also other techniques of measurement of bulk density, which are stated in the ASTM C373.

c) Theoretical density is referred to as the maximum value of bulk density that can be theoretically achieved when the ceramic material is absolutely densified. It is a density of a pore-free material, which contains crystalline phases exclusively. It represents a reference value to which the real bulk density is compared to. The difference between theoretical density and bulk density is equal to the amount of porosity present in the ceramics. In order to successfully calculate theoretical density, crystallographic density as well as the volume of each solid phase, have to be known.

3.1.2.2 Porosity

Porosity is a very important parameter to determine. The presence of open porosity and its distribution across the bulk material is of great importance because it affects mechanical, physical, electrical and many others of its properties. Open porosity is commonly detected by mercury porosimetry. Modern mercury porosimeters are equipped with software allowing the calculation of useful parameters, such as the percentage of porosity versus pressure, pore channel diameter, and many others.

Thermal properties (conductivity, expansion, heat capacity, etc.) and mechanical properties (such as elasticity, tensile strength, Poisson´s ratio, fracture toughness, etc.) are also of great importance, however, they won´t be discussed any further in this work as they are of a lower degree of relevance for this thesis purpose.

3.1.3 Oxide ceramics

Oxide ceramics is referred to as technical ceramics of a simple oxide-based microstructure. It is characterized by high strength, hardness and corrosion resistance. [12], [13]

The aim of this thesis is to describe and characterize the surface of most commonly used oxide ceramics, such as alumina (Al_2O_3), zirconia (ZrO_2), hydroxyapatite and titanium dioxide (TiO_2), by determining surface tension on their surface from water contact angle measurement.

3.1.3.1 Powder preparation and sintering process

Ceramic powder preparation include, for example, grinding, sieving, mixing, drying, etc. By sieving the ceramic powder is freed of large particles and agglomerates. According to the required parameters of the resulting powder, the appropriate technology of preparation is selected. The grinding process may be provided as a wet or dry process.

Forming may be performed by uniaxial pressing or isostatic pressing. Other methods include suspension casting, direct consolidation or tape-casting. For materials being in a plastic state, techniques of injection molding or extrusion may be used as well. Further forming methods include 3D printing or direct jet printing etc. [12]

Generally, sintering processes are divided into various categories, depending on the type of the system. Solid-state sintering is a thermal process in which particles of the ceramic powder (also referred to as 'green body') are heated to a given temperature to join together and reduce porosity. The sintering temperature varies among materials, its usual value ranges between 50% and 80% of materials' melting temperature, or, more accurately – $0.7T_m$ (melting temperature) – thus, the ceramic powder does not melt during the process. [12]

Melting temperatures of oxide ceramics mentioned in this thesis are given in a table below.

Tab. 3: Melting temperatures of selected ceramic oxides [38], [39], [40]

Oxide ceramics	*Melting temperatures [°C]*
Al_2O_3	*2072*
ZrO_2	*2715*
TiO_2	*1843*
Hydroxyapatite	*1670*

Densification of the whole body is driven by diffusion mechanisms. The process of solidification and densification is schematically shown in the figure 1. Changes in relative density over sintering time define three different stages of densification and form a well-known densification curve. [41]

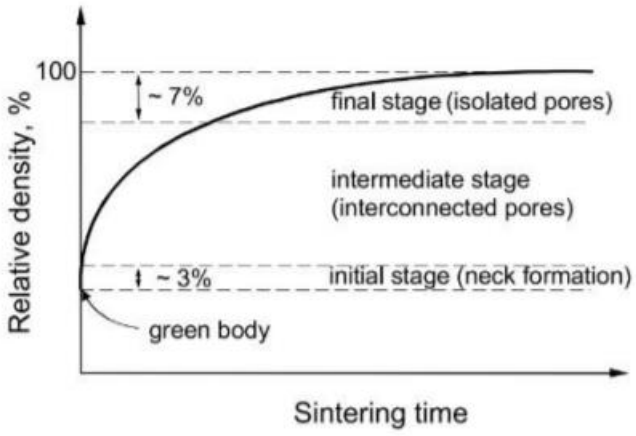

Fig. 1: Relation between relative density and sintering time – densification curve

Often, it is impossible to achieve the required density or microstructure by solid-state sintering (SSS). More suitable method in terms of achieving the desired properties and structure, is referred to as liquid-phase sintering. This process is similar to the SSS. It consists of using an additive to form a small amount of liquid phase between the particles of green body and thus improve the diffusion process and mass transfer to the porous areas. [12]

However, required porosity (or density) may still not be achieved. Further improvement of physical properties or microstructure may be achieved by applying external pressure during the sintering process – by pressure sintering.

3.1.3.2 Alumina, Zirconia, Titanium dioxide and Hydroxyapatite

This chapter offers a basic overview of materials used to perform the experiment that is further described in the experimental part of this thesis.

Al_2O_3 – Alumina (or aluminum dioxide) is prepared by Bayer´s process out of bauxite – a mixture of gibbsite, boehmite a diaspora with a dose of impurities such as silica (SiO_2), iron oxide (Fe_2O_3) and titanium dioxide (TiO_2). A simpler and energetically more favorable process is a direct extraction from natural corundum, which is, unfortunately, less abundant than bauxite. [13]
Al_2O_3 may appear in various purities ranging from 85%-99.9%, in the field of research the purity values can be even higher. Those are usually obtained using the sol-gel process. Other ways to obtain Al_2O_3 of high purity are precipitation, gas phase synthesis, hydrothermal synthesis, pyrolysis or laser ablation. [13]

ZrO_2 – is another wide-spread ceramic material. It is characterized by its high melting point of 2710°C and its structure. Zirconia is produced out of mineral $ZrSiO_4$. ZrO_2 is a polymorphous oxide and the most durable ceramic oxide. [14]
Zirconia ceramics show excellent chemical and corrosion resistance, excellent fracture toughness and wear resistance. Its application field is large – from pressure valves through bioimplants to components of chemical and mining industries. Especially in combination with Y_2O_3 it features high electrical conductivity. [14]

TiO_2 – titanium dioxide is another commonly researched oxide and one of the most published materials used for creation of nanosurfaces. An inexhaustible number of structures with different geometric parameters can be created depending on the given conditions.
Titanium dioxide itself is an insoluble, inert and non-toxic white powder with a very high melting point of 1800°C. It occurs in three crystalline structures: in the form of rutile, anatase and brookite. In addition to its use in many industries, it also features great biocompatibility, therefore TiO_2 nanostructures are often used as a top layer of a titanium implant. [15], [16]

Hydroxyapatite – also known as HA or Hap with a chemical formula $Ca_{10}(PO_4)_6(OH)_2$, is commonly found in nature in the form of the phosphate mineral apatite, in various colors – colorless, white, grey, yellow, greenish or brown. The pure hydroxyapatite powder is white and features great biocompatibility and bioactivity.

Some of the properties of above-mentioned ceramic oxides are resumed in tables 2 and 3. The knowledge of melting points (temperatures) is essential to correctly determine the range of sintering temperatures. Values of crystallographic densities are necessary to evaluate theoretical density. The last one is later compared to the real experimental density obtained throughout the measurements.

3.2 Surface characterization of ceramic materials

3.2.1 Wettability

The spreading tendency of liquid on a solid surface is referred to as wettability. It is determined by measurement of the contact angle between the substrate and the tangent that is drawn at the triple point (where 3 phases – solid, liquid, and gas – meet).
Wettability of a liquid on a solid is characterized by the degree of wetting as well as by the wetting rate. The degree of wetting is determined by the contact angle between the liquid and the solid substrate.

Right after the water droplet is deposited on the surface of a substrate, various phenomena can be observed independently or simultaneously. If the drop spreads along the whole surface of the substrate and forms a thin layer on the surface, it is known as “complete wetting”. The spreading may also be incomplete and occurs when the drop spreads only partially. There is a possibility that the drop does not spread at all or spreads only a little. This is because the surface of material is highly lyophobic. [8], [17], [18]

Figure 2 shows both water-unwetted and water-wetted surface, on the left and on the right, respectively.

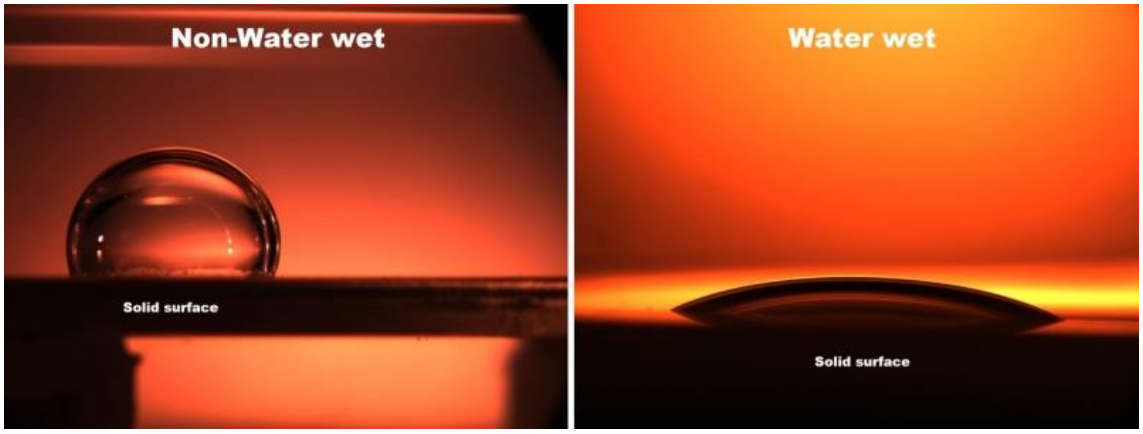

Fig. 2: Wetting of solid surfaces [43]

Generally, two types of wetting may be observed, depending on the reaction between the liquid drop and the substrate material. If there is no reaction between the liquid and the solid, it is usually referred to as non-reactive wetting, whilst if the solid and the liquid react with one another, it is referred to as reactive wetting. The droplet may be consumed by the surface of the substrate by chemical reaction or diffusion. Accordingly, the wetting process is affected by many factors. Except for the phenomena stated above, the wetting process may be affected by other factors. During the spreading process, the drop of liquid may evaporate or solidify due to the higher or lower temperatures, respectively, or because of the volatility of the substance. The nature of the substrate is very important as well. The porosity of the substrate usually results in adsorption and consecutive absorption of the liquid drop by the substrate. [8]

3.2.2 Surface tension and surface energy

Surface tension σ is defined as a force acting perpendicular to the length of the imaginary surface cut, divided by its length, as follows:

$$\sigma = \frac{f}{l} \quad (N \cdot m^{-1}), \tag{6}$$

where: σ stands for surface tension ($N \cdot m^{-1}$)
f is the acting force (N) and
l is length (m).

Consequently, additional energy is necessary to increase the surface area.
Generally, surface tension is also referred to as the areal (surface) density of surface energy.
The surface tension is a result of the asymmetry of the surface. Atoms or molecules in the bulk material are surrounded by other atoms from each side, thus the forces from the neighboring atoms are mutually canceled.
However, particles on the surface are surrounded by atoms or molecules from one side only (from the half-space of the bulk material). Therefore, the resultant of intermolecular forces acting on the particle is non-zero and is headed towards the bulk material. It is referred to as cohesion pressure. Cohesion forces are short-range because they are weaker than gravitational, electrical or electrostatic forces between atoms, thus the cohesion pressure manifests only in a thin surface layer of a width of several angstroms.
In order to increase the surface area, some atoms or molecules located in the volume of the solid, have to be moved towards the surface. As soon as the particle approaches the surface, it has to surmount the cohesion pressure that starts to act once the particle is only a few angstroms away from the surface. It is equivalent to the amount of work that needs to be done to increase the surface energy. Every particle that moves from the inside to the surface raises the surface energy and contributes to the surface tension.
On the other hand, in order to decrease the surface energy, particles have to leave the surface towards the volume of the material. Every leaving particle is accelerated by the

cohesion pressure. Afterward, the kinetic energy obtained due to this acceleration is dissipated in the volume and contributes to the energy of the volume at the expense of the surface energy.

Surface tension is affected by many factors, such as temperature or chemical composition. It decreases with rising temperature. Moreover, the surface is usually enriched by the components contributing to the decrease of surface tension.
Surface tension is also influenced by the crystallographic orientation of crystallites on the surface. [7]

3.3 Measurement of surface tension (surface energy)

3.3.1 Contact angle

Measurements of contact angles are widely provided in order to determine the character and properties of a solid surface. It is also important when examining the interactions between solids and liquids. The measurement itself is very simple, though the interpretation of results may be more complex since there exists a certain correlation between the contact angle, wettability and adhesion. [8], [9], [22]

A droplet of a probing liquid – water – is dropped on a solid surface. After a short period of time, the liquid comes to rest and makes an angle with the solid surface, as shown in the Fig. 3.

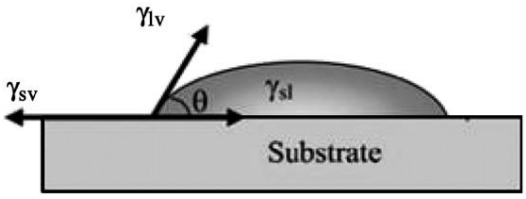

Fig. 3: Water droplet deposition on solid surface [8]

There are three different phases present in the system – the solid phase of the substrate, the liquid phase of the droplet and the gaseous phase of ambient air. At the point of contact of these three phases, a drawn tangent defines the angle which is referred to as a contact angle.
Before the droplet comes to the equilibrium state, it spreads along the surface with a driving force determined by a following equation:

$$F_d(t) = \gamma_{sg} - \left(\gamma_{sl} + \gamma_{lg} cos\theta(t)\right), \tag{8}$$

where the γ_{xy} terms stand for the interfacial tensions between phases.
After the equilibrium state is reached, the driving force is equal to zero, which leads to the Young´s equation below:

$$\gamma_{sg} - \gamma_{sl} = \gamma_{lg} cos\theta(t) \tag{8}$$

Moreover, work of adhesion W_{sl} was defined by Dupre, leading to a following equation:

$$W_{sl} = \gamma_{sg} - \gamma_{sl} + \gamma_{lg} \tag{9}$$

This variable is defined as a work performed per unit area of the interface in order to separate one phase from another.
The combination of the driving force formula and the Dupre´s equation results in the Young – Dupre formula:

$$W_{sl} = \gamma_{lg} \, (1 + cos\theta) \tag{10}$$

For a given value of the tension between the liquid phase and the gaseous phase, an inverse proportionality is observed between the contact angle and the solid-liquid adhesion. Different values of the contact angles lead to different wetting behavior of the surface. A contact angle of 180° indicates zero adhesion between the liquid and the solid substrate. As the value of the contact angle decreases, the conditions change from non-wetting to completely wetting. A given liquid is assumed to wet the surface of a solid if the contact angle is smaller than 90°. In this very case, the interfacial tensions are equal. On the other hand, a contact angle greater than 90° indicates that the surface is not wetted by the given liquid. [8], [23], [24]

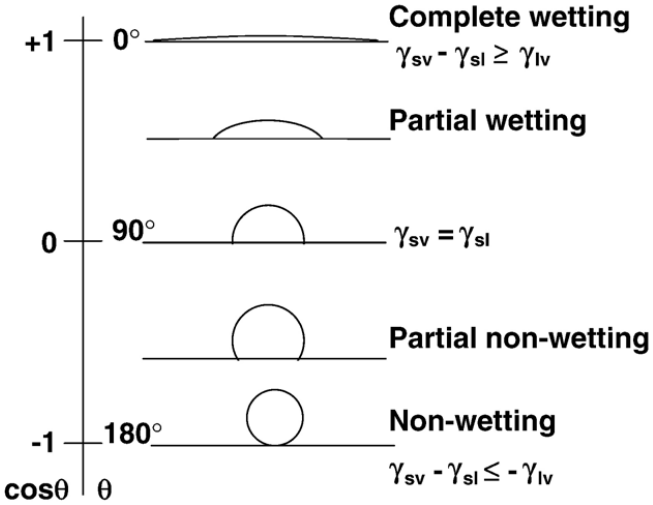

Fig. 4: Relation between contact angle and wetting [21]

A figure above illustrates this statement perfectly. However, the non-wetting conditions are very difficult to be achieved.

In the case of complete wetting, the contact angle is equal to zero and the work of adhesion reaches the value of $2\gamma_{lg}$. Physically, it represents the energy needed to keep the two phases close to one another. [8], [27]

Since there is a considerable number of parameters affecting the measurement process, a large scatter of contact angle values is obtained across various resources. Not only properties of substrate, such as the roughness and heterogeneity of surface, but also the viscosity, temperature and volume of the flowing liquid are important to credibly determine its value. Hence, it is necessary to establish a reference value, referred to as equilibrium contact angle. This one is formed under the equilibrium conditions between an ideal solid substrate and a non-reactive liquid. A term of intrinsic contact angle defines an angle obtained on a completely net surface, with no contaminating films or adsorbed particles on the surface.
The contact angle resulting from the Young´s equation is known as Young contact angle and is determined for homogenous, smooth, rigid and insoluble surface under the equilibrium conditions. [8], [19], [20]

Although, ideal conditions are impossible to be reached. Consequently, the actual measured angle is referred to as apparent contact angle, shown in the figure 5 below.

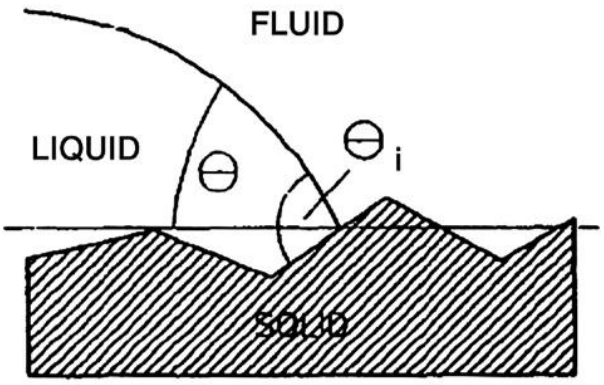

Fig. 5: Apparent contact angle [19], [20]

Furthermore, the apparent contact angle may be measured on a rough, but homogeneous surface. In that case, it is referred to as Wenzel angle. Oppositely, an angle measured on a smooth, but heterogeneous surface is known as Cassie angle. [9], [19], [20]

All of the above-mentioned angles are determined in the equilibrium state, when the liquid is not spreading along the surface.

However, given that the solid surface may be inclined, the equilibrium state is not achieved. Dynamic conditions lead to a time dependent contact angle, also called instantaneous or dynamic contact angle. In this case, the measured angle is composed of two components: an advancing and a receding part, shown in the figure below.

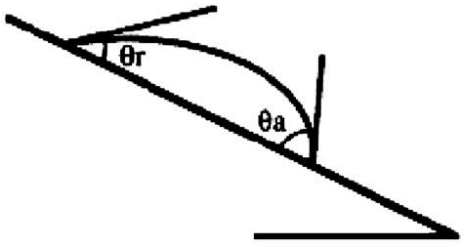

Fig. 6: Dynamic contact angles on a tilted surface [25]

A further explanation should be provided to define both terms: an advancing angle is formed when the droplet of liquid proceeds towards the gaseous phase (down the inclined plan), while the receding angle is formed when the interface leaves the gaseous phase. The final contact angle is determined from the metastable state at the point where the change of its value approaches zero. [8], [25], [27]

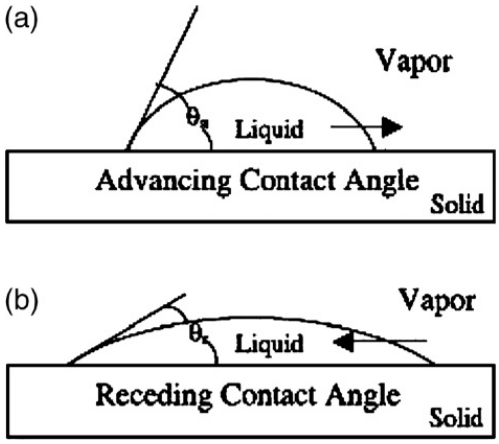

Fig. 7: Advancing and receding contact angles [25]

The contact angle on a tilted surface may also be known as a sliding angle. The regular shape of a droplet is distorted by gravity, which is illustrated in the figure 8 below. Analogically, the angles θ_{max} and θ_{min} stand for the andvancing and receding angles, respectively.

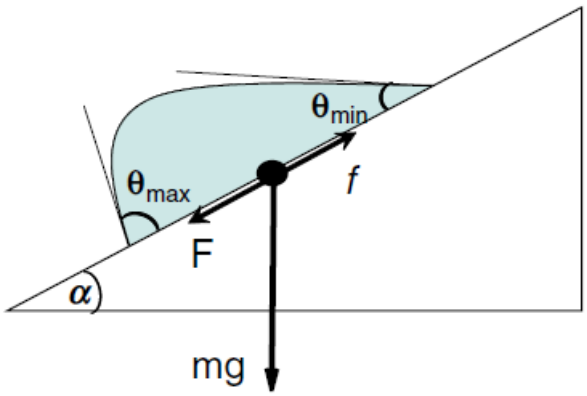

Fig. 8: Droplet distorted by gravity, advancing and receding contact angles [26]

Two different parameters are used to describe the distortion of the droplet – the driving force *F* and the frictional force *f*. The driving force (gravity) is given by the formula below:

$$F = mg \cdot \sin\alpha, \tag{11}$$

where α stands for the tilting angle, m is the mass of the droplet and g is the gravitational constant. The frictional force is much more complex and more difficult to define. A simplified two-dimensional formula is used to express and calculate its value, as following:

$$f_f = \gamma_{lg} \cdot R \cdot k \cdot (cos\theta_{min} - cos\theta_{max}), \tag{12}$$

where γ_{lg} stands for the surface tension, *R* is the length scale and *k* represents a parameter determined from experimental data.
Moments before the drop starts to slide on a tilted surface, the driving force is equal to the frictional one. Once the drop is deposited on the surface and starts to move down the inclined plan, the lead and the trail edge are formed and the θ_{min} and θ_{max} are measured. Generally, in the surface and interface science literature, the above-mentioned angles were claimed to be equal to the receding and advancing angles, respectively. However, recent findings and experimental data showed a certain difference between their values, indicating a contact angle hysteresis. Supposing the equality between the θ_{min} and θ_R, and θ_{max} and θ_A, a linear relation should be observed between $sin\alpha$ and $cos\theta_R - cos\theta_A$. Although, their dependence is not linear. It is due to the many approximations provided by deriving the equation of the frictional force. [8], [9], [26]

3.3.1.1 Contact angle hystereris

Generally, the origin of the hysteresis phenomenon comes from the existence of mechanisms that exhibit irreversible transition between states.
For a single droplet of liquid, multiple contact angles may be measured depending on the conditions of the experiment. This phenomenon is referred to as a contact angle hysteresis. The highest possible contact angle is thought to be the advancing one, when the drop moves towards the gaseous phase, mostly observed on tilted surfaces. On the other hand, the lowest angle is claimed to be the receding contact angle formed at the trial edge of the moving droplet. The hysteresis is also defined as the difference between the advancing and the receding angle.

The existence of hysteresis is conditional to the external experimental conditions such as roughness and homogeneity of the surface or the adsorption of particles on the surface of solid. The amount of adsorbed particles is proportional to the size of the hysteresis. The phenomenon of adsorption of organic particles will be studied in detail in the next chapter.

It is necessary to state that the contact angle hysteresis is not a direct measuring instrument of adhesion nor wettability of the given surface. [8], [26]

Although a correlation between the hysteresis and drop mobility has been suggested. According to many research groups, the size of hysteresis is indirectly proportional to the drop mobility and thus to the sliding angle.

3.3.1.2 Contact angle measurement

Evaluation of the wettability of a given surface has been provided by various direct or indirect methods. Some of the commonly used methods discussed in this chapter are stated in the table below. The table contains a brief summary of the advantages and disadvantages of given methods as well as their short characterization.

Tab. 4: Different wetting characterization methods [27]

Method	Characterization	Advantages	Disadvantages
Direct methods			
Sessile-drop	Capture of images of a droplet and their mathematical evaluation	Simple Small volumes of water Small surface areas	Susceptible to errors Time consuming Impurities in water
Tilting plate	Measurement from the leading edge and trailing edge of an elongated drop	Very quick method	Measured angles do not exactly correspond to the advancing and receding contact angles Measurement depends on the drop volume
Wetting balance			
Indirect methods			
Wilhelmy plate	Dipping of the solid surface into the water and determination of contact angle from the measured force	Operator errors are likely to be avoided Easy automation Quick method	Impossible to visually follow the wetting process Necessity of composition and morphology homogeneity

Among the stated methods of wettability measurement, sessile-drop technique consists of measuring of the contact angle itself. Figure 9 introduces the measuring apparatus for this technique: it requires a camera to capture photos of deposited drops, a light source and an adjustable sample stage.

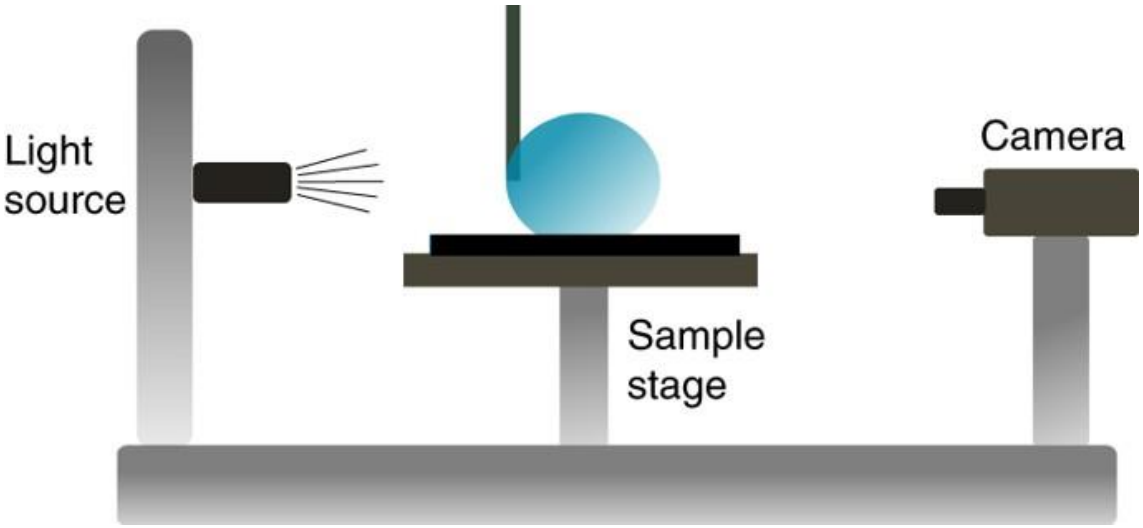

Fig. 9: Experimental setup for sessile-drop technique – sessile-drop goniometer [44]

Sessile-drop method is commonly used thanks to its simplicity. Additionally, it provides a reliable source of the surface behavior in the real conditions. A given volume of liquid is dropped on the surface of a solid substrate in order to spread to a certain extent. The images of the drop are taken and processed subsequently. The analyze of the taken pictures is provided by fitting a mathematical expression to the shape of the drop. Then, the slope of the tangent drawn from the triple point is calculated to determine the value of the contact angle. Supposing that the measurement is provided accordingly, the droplet is symmetric about the *y* axis and is in a steady state, the results should be reliable and reproducible. The value of contact angle obtained from this measurement can also be used to evaluate the wettability of the surface.

However, it is likely that the surface of the substrate is slightly inclined or tilted, which causes that the droplet of water deforms due to the effect of gravity. In that case, symmetry about the *y* axis is not achieved and both advancing and receding contact angles have to be measured to assure reproducibility and reliability of results. [27]

3.4 Organic adlayer on inorganic materials

The surfaces of metals and ceramic oxides featuring high surface energy are usually contaminated with organic molecules. The presence of adsorbed particles is a major concern, because it may contribute to the changes of properties of the surface, such as adhesion and wettability. These surface characteristics are determined by water contact angle measurement (WCA), which provides a very convenient and rapid technique for wettability evaluation. This method is highly surface specific and reliable when it comes to its sensitivity – it usually exceeds the sensitivity of electron spectroscopies. [10], [11]

Because the presence of adsorbed particles directly affects above-mentioned characteristics, it is essential to remove them prior to any further processing or surface modification and treatment. [10], [28], [29]

Thoroughly cleaned surfaces are characterized by lower values of contact angles. As the surface is exposed to the ambient air, organic particles naturally present in the laboratory environment start to adsorb on the surface. Being of a hydrophobic nature, adsorbed organic contaminants are responsible for a decrease of surface hydrophilicity and indeed for an increase of contact angle values. [11]

However, it is important to note that higher values of contact angles do not necessarily imply the adsorption of the contaminants on the surface. All clean oxide surfaces should not be assumed to be highly hydrophilic, neither. [10]

Various chemical or thermal surface treatments, as well as the presence of contaminating particles in the manufacturing process may influence the hydrophilicity or hydrophobicity of a given surface. Also, an aptitude of organic particles to adsorb on an inorganic surface may be lower or higher depending on a specific thermal or chemical modification of surface.

The rate of increase of the WCA value is affected by the nature of the substrate as well as by the surrounding environment. According to the literature, the adsorption of contaminants is more effective and way more faster under high vacuum than in the ambient air. [10]

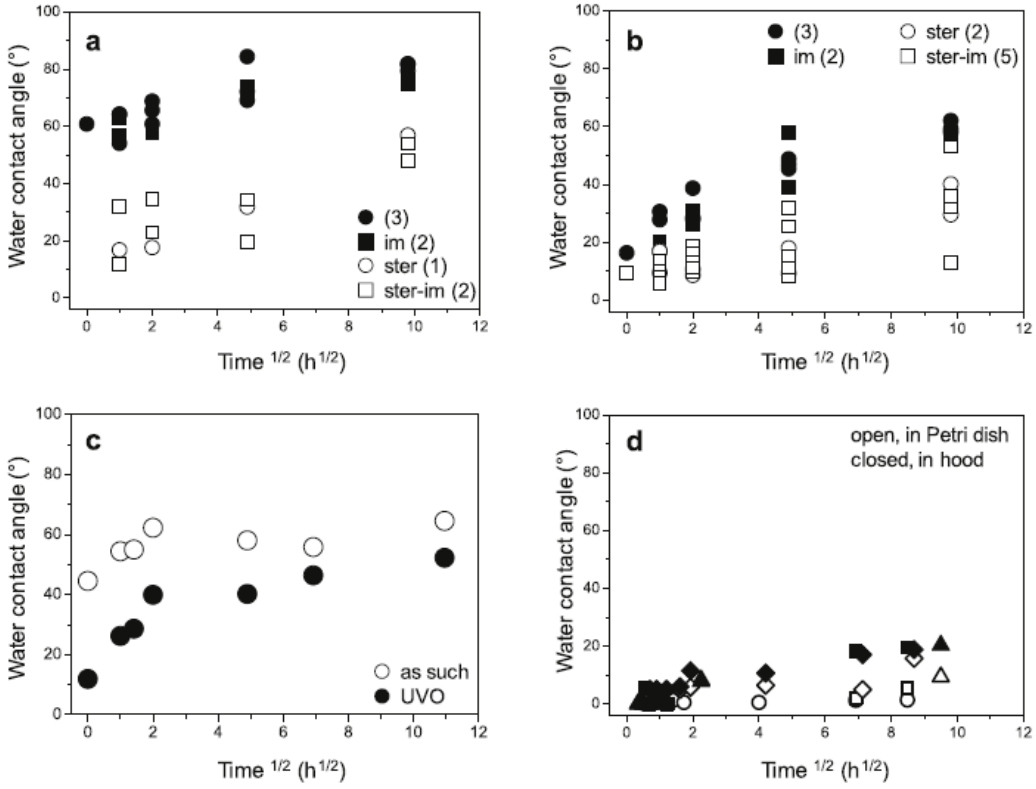

Fig. 10: Evolution of WCA over storage time in ambient atmosphere [10]

The evolution of WCA over time is shown in the Figure 10. Pictures (a), (b), (c) and (d) show that WCA evolution is a function of storage time in ambient atmosphere. Longer exposure to the ambient air clearly results in the increase of WCA. Moreover, cleaned surfaces with RBS (picture b), with or without additional UVO treatment, either sterilized or not, result in the decrease of the contact angle measured right after the treatment. However, over a period of time, WCA starts increasing again. Picture (c) represents samples cleaned with ethanol, with or without further UVO treatment and picture (d) shows WCA of samples either left in a Petri dish or exposed to the air flow in the laboratory hood.

According to the literature and references stated above, WCA values change over time regarding the environment in which they are left in and also regarding the cleaning or treatments performed on the studied surface. As the contaminating compounds demonstrably decrease hydrophilicity of the surface, experimental measurements of WCA under different conditions could credibly determine the most efficient and favorable way of their removal from the surface.

Many methods are used to detect and analyze the organic layers on inorganic surfaces, where X-ray photoelectron spectroscopy (XPS) is considered to be the most suitable one. Other methods, such as AES (Auger Electron Spectroscopy), TOF-SIMS (Time-of-flight Secondary Ion Mass Spectroscopy), LEIS (Low-Energy Ion Scattering) and Raman Spectroscopy, are convenient as well and are described in more detail in the following subchapters. [10]

Water contact angle measurements are provided to assess wettability and surface energy, while the XPS method provide us with the quantitative information on the chemical nature of the contaminants (elemental composition).

3.4.1 Surface analysis methods

Methods for detection and analysis of surface contaminants that are mentioned above are altogether capable of examining sub-monolayer films and sub-micrometer particles. Each of these methods suits best for a specific contaminant studies. To correctly choose the most suitable method, one must have some information about the nature of the substrate as well as about the properties of contaminating compounds. At least minimum knowledge regarding the adsorbent’s volatility, shape, size or morphology is essential in the selection process. Furthermore, expected results can also affect the right choice of the analysis method. It is important to consider whether qualitative or quantitative results are expected (e.g. compound identification, elemental composition, etc.). The choice of right analysis method is though rather limited. All the criteria that possibly influence and limit the choice of a specific method, are summarized in the detailed table in the Fig. 11. [11]

Method	AES	LEIS	TOF-SIMS	XPS
Material	Conducting or semi-conducting solids. Insulators are very difficult	Any solid	Any solid	Any solid
Information	Elemental. Oxidation state or chemical bonding in select cases	Elemental	Molecular weight, chemical bonding, and elemental	Chemical bonding, oxidation state, and elemental
Quantitative Analysis	Yes, best with standards	Yes, standards not required	Only with standards	Yes, best with standards
Minimum Analysis Size	10 nm diameter	100 μm diameter	~2 μm diameter for organic analysis, 50 nm diameter for inorganic analysis	10 μm diameter
Sampling Depth	5–25 monolayers	1 monolayer	1–3 monolayers	5–25 monolayers
Detection Limit	0.1–1.0 at.%	1×10^{9} to 5×10^{15} atom/cm^2	1 ppma, 1×10^{8} atom/cm^2	0.01–1.0 at.%
Imaging	Yes, rapid	Yes, in principle	Yes, rapid	Yes
Depth Profiling	Yes, rapid	Yes	Yes, rapid	Yes
Major Limitations	Electron beam damage. Charging of insulating samples.	Poor sensitivity for low mass atoms. Poor resolution between high mass atoms.	Ion yields vary by orders of magnitude. Standards needed for quantitative analysis.	Relatively large analysis area. Analysis is often time consuming.

Fig 11: Selected properties of methods for surface analysis [11]

3.4.1.1 AES – Auger Electron Spectroscopy

AES technique is one of the most commonly used method for surface analysis. Except hydrogen and helium, it can detect all the other elements. This incapability comes from the principle of this method, which is displayed in the figure below.

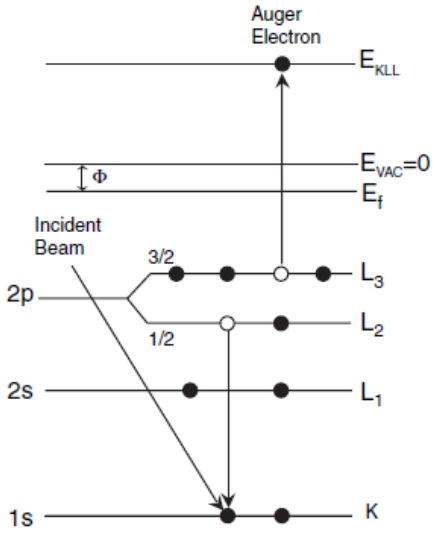

Fig. 12: Schematic diagram of Auger Electron emission process [11]

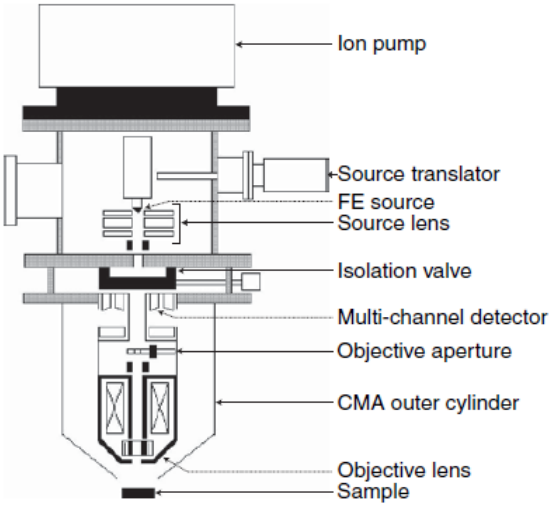

Fig. 13: Scheme of AES chamber [11]

The sample is bombarded by a high energy electron beam which causes that the core electrons of all atoms within a depth of 1 μm are removed to form a vacancy. The vacancy can be filled with an electron from an outer shell, which is accompanied by emission of a second outer shell electron and by the release of energy. [11]

This quantitative surface analysis method is sufficient enough to determine and identify particular elements from which the electrons were emitted, but it cannot determine the chemical or oxidation-state of the atom. Compound identification by Auger Electron Spectroscopy is hence derived from the relative abundances of particular elements. [11]

3.4.1.2 Time-of-Flight Secondary Ion Mass Spectrometry

Despite the initial rejection of this analyzing method, ToF-SIMS evolved to a commonly used technique for detection of organic and inorganic contaminants on the surfaces. The principle of the method is quite simple. It consists of the bombardment of the sample with high-energy ions which results in the emission of secondary ions. The analysis comprises the measurement and evaluation of time that secondary ions need to fly from the sample to the detector. This technique is simple in its principle, yet it is more difficult to produce and maintain an ion pulse with required parameters. Measurements of secondary ion flight times are not the simplest, neither. [11]

ToF-SIMS generally meets almost all the requirements for identification of organic and inorganic contamination. It can detect any element of the periodic table and, what is more, all the functional groups of organic compounds, and, even molecules. One of the many advantages of this technique is that all types of materials (organic, inorganic, metallic) can be analyzed as long as they can sustain vacuum conditions. [11]

3.4.1.3 Low-energy Ion Scattering

Since its first use in early seventies, this method of surface analysis has evolved into one of the mostly used techniques for surface composition evaluation. This method studies only the very first layer of the sample surface. Disadvantages of LEIS result from the poor sensitivity to low-mass elements and low spectral resolution between adjacent high mass. [11]

Basically, it measures backscattered ions during ion-surface collisions. In most of the applications, ions $^4He^+$ are used. During the bombarding of the surface by low-energy ions, some of the ions from the sample are elastically scattered and, subsequently, pass a certain amount of their kinetic energy to the atoms on the sample surface. The principle of this analytical technique is shown in the Fig. 14.

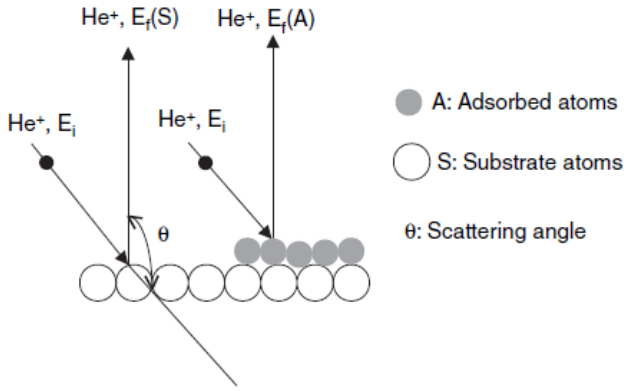

Fig. 14: Scheme of a LEIS process [11]

3.4.1.4 XPS – X-Ray Photoelectron Spectroscopy

XPS technique is, as the name suggests, based on the photoelectric effect. The effect is created by the X-ray illumination of the material which results in the emission of electrons. A scheme of the photoelectron emission process is shown in the Fig. 15.

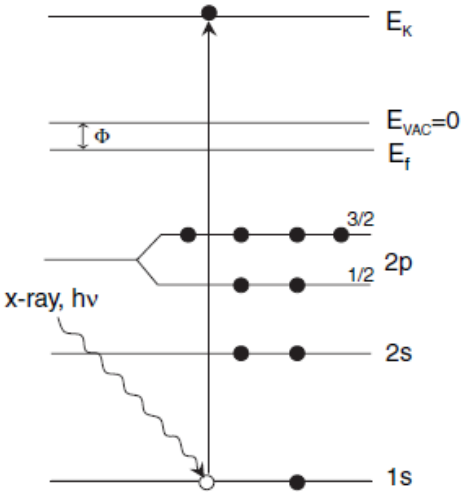

Fig. 15 Photoelectron emission [11]

The use of XPS across many fields is very extensive. The X-Ray photoelectron spectroscopy is mostly used for identification of surface composition and for studying and evaluation of corrosion, adhesion failures and cleaning methods. [11]

This technique is capable of examining both solids and low volatility liquids and both conductive and insulating substrates. Some possible limitations may originate from the detection limits and from the minimum analysis area.

XPS is one of the most suitable methods for analyzing the adsorbed organic molecules on inorganic surfaces, because it can detect any element except hydrogen and helium. Inorganic compounds such as ceramic oxides studied in the experimental part of this thesis are prone to be coated by organic adsorbents, thus, carbon is often detected on their surfaces. Detection of carbon on the surfaces of inorganic substrates therefore indicates an adventitious contamination, therefore XPS analysis is referred to as the most demonstrative methods of organic compounds adsorption on surfaces. [10], [11]

3.4.2 Volatile organic compounds (VOC)

Inexhaustible amount of organic compounds, varying in their abundance, have been detected in the ambient air. The most numerous, yet less reactive ones, with ratios ranging from hundreds of parts per million down to some parts per million – such as carbon dioxide, methane and carbon monoxide – are excluded from this overview. This chapter focuses on carbon-containing gases whose abundance in the atmosphere varies from some parts per billion (ppbv) to some parts of trillion (ppt). Despite many attempts to classify

these compounds, the term of "volatile organic compounds (VOC)" has been set only recently with no general quantitative definition. VOC are therefore considered to embrace all the species under approximately 10 ppbv relevant to atmospheric chemistry – meaning that they participate in atmospheric photochemical reactions. [30], [31]
More precisely, an organic compound is considered to be a VOC if following parameters are fulfilled: the organic compound has a vapour pressure higher than 10 Pa at 25°C, a boiling point of up to 260°C at atmospheric pressure and has at maximum 15 carbon atoms. [30]

3.4.2.1 Sources

Organic compounds are being emitted from wide range of processes and activities of daily life. Every human activity results in emission of carbon compounds such as alcohols, alkanes, esters, carbonyls, aromatics, ethers and amides. Except of emission originating in everyday activities and production, organic gases are naturally emitted from the Earth´s vegetation. Carbon compounds, especially their reduced forms such as terpenes and isoprene, are emitted during photosynthesis. More accurately, the abundance of emitted organic gases as well as their exact composition are specific to the particular plant. The nature and the amount of organic compounds are also given by the external conditions, being temperature, moisture and light level. [30]

Generally, most of the organic compounds emitted to the atmosphere are of a biogenic (Earth´s vegetation) or anthropogenic (human activities) nature. Each of the contributing parts is further discussed in the following chapters.

3.4.2.2 Anthropogenic sources of VOCs

Most organic compounds originating from human activities are emitted due to the exploitation of fossil fuels such as coal, oil and gas, from technological sources and burning of biomass. Not only the production of liquid fossil fuels, but also their distribution and storage lead to massive emissions of hydrocarbons into the atmosphere. Coal production, as well as crude oil production, are responsible for significant emissions of alkanes, mostly methane, ethane and propane. Significant amount of organic gases is emitted during their processing. The contribution of particular processes is dominated by catalytic cracking, followed by coking and asphalt blowing. Furthermore, organic gases emissions can result from leaks and evaporation during operational procedures or from the equipment itself. [30]

According to their chemical nature, three different groups of VOCs can be distinguished:

- non-methane hydrocarbons (NMHCs)
- oxygenated hydrocarbons (OVOCs)
- halogenated hydrocarbons (for example chlorofluorocarbons [CFCs] or hydrofluorocarbons [HFCs]).

However, certain groups of VOCs can be emitted from both anthropogenic and biogenic sources. NMHCs (alkanes and alkenes except of methane) are dominantly emitted by anthropogenic sources, yet they can come from natural sources as well, e.g. from soils and oceans. OVOCs like ketones and alcohols (e.g. acetone, methanol) are, on the other hand, mostly coming from vegetation, but can be emitted from fossil fuels exploitation and combustion as well. [30], [45], [46], [47], [48]

As mentioned above, not only the exploitation of fossil fuels, but also their storage and distribution are significantly contributing to the emission of hydrocarbons into the atmosphere. Ethane, being the simplest alkane (excluding methane), is the most abundant alkane whose emission is mainly originating from the petrochemical processes. Similarly, propane is also emitted during the distribution and storage of natural gas and petrochemical products. Higher alkanes ($C_4 – C_5$) are present due to the evaporation of fossil fuel and due to exhaust. As the chain length increases, evaporation is of a lower relative importance due to the lower vapor pressure of high molecular alkanes, therefore their amount in the atmosphere is significantly lower. [30]

Because of an incomplete fuel combustion, alkenes are also emitted in a significant amount. Again, the most abundant alkenes are the simplest ones, yet their presence in the air is decreasing rapidly due to their higher reactivity. Relative lifetimes of particular organic compounds emitted into the atmosphere are summarized in the Tab. 5.

In polluted environments, alkynes, such as ethylene, are present as a result of an incomplete combustion as well. However, alkynes can also come from biomass burning. The presence of different types of organic compounds varies across the planet, accordingly to the urban or rural areas.

Mostly all of the VOCs are emitted from fossil fuel and petrochemical industry, aromatic VOCs not being an exception. Another significant pollutants are xylene and toluene, since they are used as solvents as well. [30]

Incomplete combustion also leads to the emissions of OVOCs, but since their main sources are of a biogenic nature, they will be further discussed in the following chapter.

Tab. 5 Relative lifetimes of particular organic compounds emitted into the atmosphere [30]

Category	*Example*	*Average lifetime in atmosphere*
Alkanes	*Ethane*	*2.5 months*
	Propane	*2.5 weeks*
	n-pentane	*4 days*
Alkenes	*Ethene*	*1.5 days*
	Propene	*11 hours*
	1-butene	*10 hours*
Aromatic compounds	*Benzene*	*2 weeks*
	Toluene	*2 days*

The presence of particular VOCs in the atmosphere is temporary and follows the average lifetimes stated in the table above. Once they are emitted, they take part in various photochemical processes which subsequently lead to their removal. Most of the VOCs are oxygenated by atmospheric radicals OH, O_3, NO_3 and Cl, other VOCs, especially OVOCs, are directly photolyzed thanks to their absorption of radiation. [30]

In the meantime of their presence in the ambient air, volatile organic compounds are susceptible to adsorb on surfaces. According to their average lifetime in the atmosphere, some of the VOCs can represent important pollutants to the objects' surfaces. Adsorption of different VOCs to the surfaces of materials can lead to changes in properties of the surfaces, such as adhesivity and hydrophilicity. These changes can be easily described by surface energy measurements provided by contact angle evaluation. Experimental part of this thesis focuses on the assessment of changes of surface properties using water contact angle measurements on surfaces of different oxide ceramics with different physical, chemical and surface properties. [30]

3.4.2.3 Biogenic sources of VOCs

Earth´s vegetation, oceans and soils are equally important source of organic compounds in the atmosphere. The very first compounds to be found important to the atmospheric composition, were isoprene and terpenoid compounds. Generally, biogenic volatile organic compounds can be categorized by their chemical speciation introduced in the following Tab. 6. It also summarizes the average lifetimes of particular compounds in the atmosphere. In terms of abundance of particular contributors, the table is organized in a descending order. Isoprene and terpenes are emitted in large amounts. They are followed by oxygenated VOCs (oxVOCs) and very reactive biogenic VOCs (VR-BVOCs) with very short average lifetimes. [30]

Tab. 6: Average lifetimes in the atmosphere of biogenic volatile organic compounds

Category	*Example*	*Average lifetime in atmosphere*
Isoprenoids	*Isoprene*	*3h*
Terpenoids	*Pinene*	*4h*
oxVOCs	*Acetone*	*Weeks – months*
VR-BVOCs	*Caryophyllene*	*Minutes – hours*

The majority of the biogenic VOCs comes from the terrestrial vegetation, being trees, plants and grasses. Soils and oceans represent another biogenic source, yet their importance is lower compared to that of an Earth's land vegetation.

Forests as such represent the major source of biogenic VOCs. Again, similarly to the diversity of emissions by anthropogenic sources, certain trees can emit various organic compounds, differing in their abundance and chemical nature. Generally, the diversity can be observed between deciduous and coniferous forests, since some are considered to be the predominant source of isoprene, whilst others are mostly responsible for emission of oxygenated VOCs including methanol, ethanol, and acetone, respectively. [30]

Both type of trees are also thought to be a source of very reactive volatile organic compounds.

The emission of biogenic VOCs is dominated by forests, however, they are not the only contributors of VOCs to the atmosphere. Other vegetation such as grasslands and urban landscapes emit significant amount of isoprene and oxygenated VOCs. [30]

Small, yet not negligible amount of VOCs are emitted from oceans and soils. Compared to the overall contribution of terrestrial vegetation, the amount is much lower. Although, some specific species, e.g. hydrocarbons, halocarbons, Sulphur-containing compounds and oxygenated VOCs, are primarily emitted from oceans. Similarly to the oceanic emissions, the VOCs originating from soils are of a lower magnitude than those of the terrestrial vegetation. To determine their exact amounts and importance with respect to the overall global emission of VOCs, further research and studies are to be explored in the future.

The experimental part of this thesis was primarily focused on the changes of surface characteristics due to the adsorption of volatile organic compounds from the atmosphere. These changes were assessed by water contact angle measurements and lead to describe the influence of the adsorbed VOCs on the surfaces of different ceramic oxides. [30]

4 EXPERIMENTAL PART

4.1 Preparation of model ceramic materials – uniaxial pressing

Samples were prepared out of following ceramic powders: zinc oxide ZnO nano powder, titanium dioxide TiO_2, aluminum dioxide Al_2O_3, 3 mol% yttria stabilized tetragonal zirconia (3Y-TZP) ZrO_2 and finally hydroxyapatite $Ca_{10}(PO_4)_6(OH)_2$. All of the above-mentioned materials along with their respective labels are listed in the table 5 below.

Tab. 7: List of ceramic materials used for sample preparation

Material	*Manufacturer*	*Label*	*Theoretical density [g·cm^{-3}]*
ZnO – IAM nano powder	*Inframat Advanced Materials*	*ZN*	*5.61*
TiO_2 - P25Aeroxide 2015	*Degussa*	*TI*	*4.25*
Hydroxyapatite – SIGMA	*SIGMA*	*HA*	*3.16*
Al_2O_3 AES – 11C	*Sumittomo Japan*	*AL*	*3.95*
3Y-ZrO_2 (TZ - 3Y)	*Tosoh*	*ZR*	*6.08*

Samples were prepared by uniaxial pressing using BRIO Hranice BSML 21 uniaxial pressure machine. The shape of the samples was given by the geometry of the pressure die – they were formed as discs of a diameter of 12 mm and height of 3 mm. The amount of ceramic powder used to prepare the samples is selected accordingly – given the density of the particular ceramic powder – between 0.35 to 0.75 g. Uniaxial pressing procedure required following equipment: a pressure die of a diameter of 12 mm, 2 punches, ethanol for the cleaning process, lubrication consisting of PVA dissolved in ethanol, cleaning paper towels and 3D printed support for sample removal from the die.

Once the powders and the equipment were prepared, a customized program was set on the pressing machine depending on the given material – given the fact that each ceramic oxide needed different pressing conditions (different pressure to sustain). Specific conditions for each material are summarized in the Tab. 8 below.

As long as the pressing procedure was finished, the sample in the shape of a disc was easily removed from the die using the 3D printed support.

Tab. 8: Uniaxial pressing parameters

Material	*Mass [g]*	*Set force [kN]*	*Applied pressure [MPa]*	*Pressing time [s]*
ZnO – IAM Nano Powder	*0.75*	*3.4*	*30*	*120*
TiO2 P25 Aeroxide 2015	*0.35*	*1.7*	*15*	*120*
Hydroxyapatite – SIGMA	*0.5*	*4.5*	*40*	*120*
Al2O3 AES –11C	*0.75*	*4.5*	*40*	*120*
3Y-ZrO_2 (TZ-3Y)	*0.75*	*2.3*	*20*	*120*

4.1.1 Sintering

All the sintering processes were provided in the standard superkanthal furnace (CLASIC CZ ltd., Czech Republic) following an individual program:

- ZnO, TiO_2 and hydroxyapatite were sintered at 1100°C with a heating rate of 5°C/min, dwell time of 120 minutes at sintering temperature and a cooling rate of 10°C/min
- Al_2O_3 and ZrO_2 were both sintered at various temperatures as following:
    - ZR13 was sintered at temperature of 1300°C with a heating rate of 5°C/min, dwell time of 120 minutes at 1300°C, and a cooling rate of 10°C/min.
    - ZR14 was prepared at 1400°C following the same heating rate, dwell time and cooling rate as ZR13
    - ZR15 and AL15 were sintered at 1500°C, with a heating rate of 5°C/min, dwell time of 120 min at the sintering temperature, and cooling rate of 10°C/min
    - ZR16 and AL16 were heated up to the temperature of 1600°C with a heating rate of 5°C/min and after a 120-minutes long dwell they were cooled down to the room temperature with the rate of 10°C/min.

Apart of the above-mentioned samples, standard samples of sapphire and silica were also used for the up-coming measurements described in next chapters to illustrate and follow the changes on the surfaces. They were not prepared along with other samples used in this experiment, therefore some information including their sintering temperatures are not stated. Those samples are further referred to as "referral samples" and the measurements were provided in order to compare and confirm the changes on the materials' surfaces. These samples are listed separately in the Tab. 9.

Tab. 9:Referral samples of sapphire and silica

Material	*Label*	*Polishing*	*Thermal Processing*	*Chemical Processing*
Sapphire (Al_2O_3)	*SA*	*yes*	-	-
	SA-C	*yes*	*calcination*	-
	SA-CE	*yes*	*calcination*	*ethanol*
Silica (SiO_2)	*SI*	*yes*	-	-
	SI-C	*yes*	*calcination*	*ethanol*
	SI-CE	*yes*	*calcination*	*ethanol*

All the samples prepared by uniaxial pressing and sintered in the superkanthal furnaces are listed in the Tab. 10. It summarizes their respective labels as well as all the information about different surface treatments. Detailed description of particular processes of thermal and chemical treatments are stated further in this thesis.

Tab. 10: Summary of all sample types

Material	*Sintering temperature [°C]*	*Label*	*Polishing*	*Thermal Processing*	*Chemical Processing*
ZnO	*1100*	*ZN11*	*yes*	-	-
		ZN11-C	*yes*	*calcination*	-
		ZN11-CE	*yes*	*calcination*	*ethanol*
TiO_2	*1100*	*TI11*	*yes*	-	-
		TI11-C	*yes*	*calcination*	-
		TI11-CE	*yes*	*calcination*	*ethanol*
Hydroxyapatite	*1100*	*HA11*	*yes*	-	-
		HA11-C	*yes*	*calcination*	-
		HA11-CE	*yes*	*calcination*	*ethanol*
Al_2O_3	*1500*	*AL15*	*yes*	-	-
		AL15-C	*yes*	*calcination*	-
		AL15-CE	*yes*	*calcination*	*ethanol*
	1600	*AL16*	*yes*	-	-
		AL16-C	*yes*	*calcination*	-
		AL16-CE	*yes*	*calcination*	*ethanol*
ZrO_2	*1300*	*ZR13*	*yes*	-	-
		ZR13-C	*yes*	*calcination*	-
		ZR13-CE	*yes*	*calcination*	*ethanol*
	1400	*ZR14*	*yes*	-	-
		ZR14-C	*yes*	*calcination*	-
		ZR14-CE	*yes*	*calcination*	*ethanol*
	1500	*ZR15*	*yes*	-	-
		ZR15-C	*yes*	*calcination*	-
		ZR15-CE	*yes*	*calcination*	*ethanol*
	1600	*ZR16*	*yes*	-	-
		ZR16-C	*yes*	*calcination*	-
		ZR16-CE	*yes*	*calcination*	*ethanol*

4.1.2 Density measurements

Measurements of relative density were performed by Archimedes method using analytical scales Mettler XS 105 with measurement accuracy of 0.0001 g. Prior to the measurement, selected samples were placed under the infrared lamp for about 45 minutes to assure the removal of excessive moisture. Right after that, dry mass m_{dry} of the samples was measured. In order to remove air from the interior of the samples, the measurement has to be provided at the lowest possible pressure. Dried samples are though put in the exicator, where the pressure is lowered to 50 mbars for 30 minutes. Then the samples are immersed into the deionized water (HPLC Water, LACHNER) for another 30 minutes and are left, at low pressure, in the exicator. After half an hour, the pressure is smoothly set to rise for another 30 minutes to reach the atmospheric pressure, so that the samples could be removed from the exicator. Next, the mass m_w was measured for all the selected

samples – they were immersed into the deionized water of analytical scales, where the "wet mass" was determined. Finally, surfaces of samples were further dried and their mass m_d was determined.

With knowledge of particular masses of the samples, relative densities of every ceramic oxide could be determined using following equations.

$$\rho_{rel1} = \frac{m_{dry}}{m_w - m_d} \cdot \frac{\rho_{H_2O}}{\rho_{theor}} \cdot 100 \quad [\%] \tag{13}$$

ρ_{H_2O} stands for the density of deionized water. It is dependent on its temperature (T_{H_2O}) and is determined from equation below:

$$\rho_{H_2O} = \frac{(0{,}997 - 0{,}9984)}{5 \cdot (T_{H_2O} - 20)} + 0{,}9984 \quad [kg \cdot m^{-3}] \tag{14}$$

Relative density is progressively determined for all the measured masses in order to evaluate average relative density.

Along with the densities, volumes of open (V_O) and closed (V_C) pores can be determined as well. Their values are obtained using formulas below:

$$V_O = \frac{m_d - m_{dry}}{m_d - m_w} \cdot 100 \quad [\%] \tag{15}$$

$$V_C = \left(\frac{m_{dry} - m_w}{m_d - m_w} \cdot 100\right) - \rho_{rel1} \quad [\%] \tag{16}$$

4.1.3 Grinding and polishing

Before grinding and polishing of the surfaces, samples were mounted into the polystyrene. To mount the samples, general purpose polystyrene KRASTEN 137 was used. Samples of each kind, grouped by 2 or 3, were put into stubs with diameter of 30 mm placed on a Petri dish, as shown in the figures 16 and 17. Stubs were filled up with polystyrene, labeled, and put into the heating oven (Universal Oven UN110, Memmert) for 50 minutes at a temperature of 180°C – figure 4. Once the samples were mounted and cooled down to the room temperature, they were pulled out of the stubs to be polished.

Polishing was provided using Grinder/Polisher Tegramin 30 (TEGRAMIN) – semiautomated machine for materialographic samples preparation. Samples were put into the clamping system and polished using resin bonded diamond discs MD-Piano 80 and MD-Piano 220 (all from company Struers), respectively. Polishing process was assisted by wetting agent (water) or diamond polishing suspensions dosed automatically during the process.

Fig. 16: Labeled molds after mounting

Fig. 17: Mounting in the heating oven

4.2 Thermal etching and SEM

From each material (and each sintering temperature, if there was more), one sample was chosen for microstructure analysis. To determine the average grain size and confirm the accuracy of density measurements, surfaces were observed using scanning electron microscope (SEM- FEI Verios 460L).

To reveal the microstructure of given surfaces, samples underwent thermal etching. Samples sintered at lower temperature (1100°C) were etched at temperature of 900°C with a heating rate of 5°C/min, dwell time 30 minutes and cooling rate of 10°C/min. The rest of the samples (zirconia and alumina) with sintering temperatures of 1300°C and above, were etched at temperature of 1200°C with the heating and cooling rate of 5°C/min and dwell time of 30 minutes at etching temperature. These parameters were set with respect to the successful revelation of microstructure and minimum influence to the changes of density and average grain size at the same time. All thermal etching procedures were performed in laboratory furnaces (CLASIC CZ ltd., Czech Republic).

4.3 Surface modification

Multiple sintering temperatures for some of the materials (Al_2O_3 and ZrO_2) were chosen to follow the changes in their density and porosity that were also further assessed by microstructure analysis. Nevertheless, further chemical and thermal procedures were suggested to observe their influence on the surfaces of different materials, mostly when it comes to the adsorption of organic compounds to the surfaces.

Prior to any further thermal or chemical treatment, primary measurements of water contact angles were provided on all polished surfaces, including the referral samples.

4.3.1 Thermal processing – calcination

Samples were divided into two groups, where one of them was labeled “control group” and the other was subject to the thermal treatment of calcination. The calcination took place in the tube furnace (CLASSIC – HT1250T) in the presence of airflow following a heating rate of 2°C/min to the temperature of 800°C, then a cooling rate of 2°C/min to a

temperature of 600°C with a total dwell of approximately 16 hours. After 16 hours, assisted by an N_2 flow, samples were continuously cooled down to the room temperature.

Subsequently, right after the samples were removed from the furnace, they were placed into the deionized water to avoid any contamination of the surface from the organic compounds in the ambient air.

4.3.2 Chemical processing – cleaning with ethanol

Immediately after water contact angle measurements on calcinated samples, these were immersed into the ethanol for approximately 2 hours. Then, samples were systematically retrieved from the liquid and were left to dry in the ambient air. Given that ethanol is quite volatile, samples were almost immediately ready for measurements of contact angles on their surface. The goal of this procedure was to determine and describe the changes of surface characteristics resulting from additional surface cleaning with alcohol-based substance.

Both thermal and chemical treatment were also realized on the referral samples of sapphire and silica.

The changes of surface characteristics originating from adsorption of volatile organic compounds and demonstrated through the measurements of water contact angle on differently treated surfaces are presented in the chapter Results.

4.4 Surface characterization by measurement of contact angle

Characterization of surface was performed using the sessile-drop method. Figure 18 shows the experimental goniometer.

The basic goniometer consisted of an adjustable sample stage, a light source, and lenses connected to the camera of an embedded smartphone. The camera image was wirelessly transmitted to the computer, where the photographing process was controlled.

Sessile-drop method was performed by providing photos of deposited water droplet on a solid surface of the sample. The drop of ultra-pure deionized water (HPLC Water, LACHNER) has been deposited manually using Hamilton microsyringe showed in the figure 19 (Hamilton syringes-700 series, 0.25 ml). The precise volume of each drop had to be respected to avoid measurement irregularities caused by the effect of drop size. The volume of the droplet was set to be approximately 3 μL. As the droplet was placed, a photo was taken immediately afterwards to prevent evaporation or infiltration. Then, the surface was dried with a flow of N_2 and the procedure was repeated again. Altogether, 3-5 drops were dropped across every sample, so that at least 20 photos of water droplets were taken for each material.

Fig. 18: Experimental equipment for sessile-drop method

Fig. 19: Hamilton microsyringes [32]

4.4.1 Image processing

All the images were subsequently processed in the program called ImageJ using a plugin for contact angle measurements.

Set of points that was assigned to the outlines of the drops was interpolated by a fitting curve using “manual points procedure” plugin function. This mathematical function provided all the necessary information for contact angle determination – average contact angles were determined thanks to the tangent lines drawn automatically from the triple points.

Figure 20 shows an original photo captured by the camera during measurements. Processed image with drawn tangent lines for left and right contact angles are shown in the figure 21.

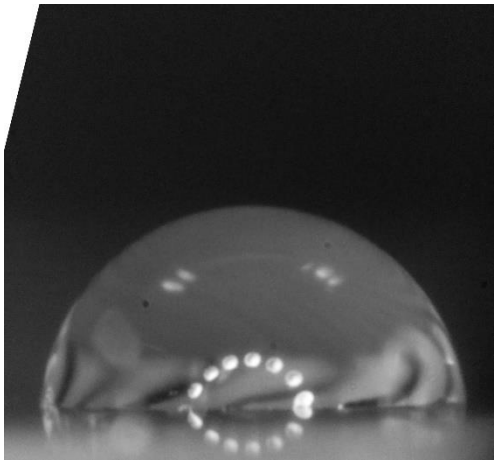

Fig. 20: Captured photography of deposited water droplet on the surface of sapphire monocrystal

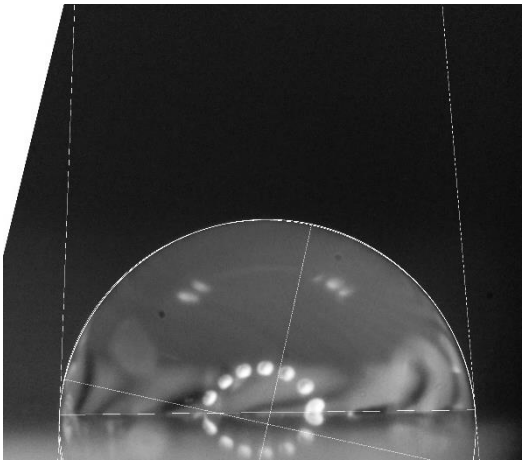

Fig. 21: Processed image of the deposited water droplet on the surface of sapphire monocrystal

Simplicity of this method may be misleading. It is important that these measurements are effectuated accurately, particularly with respect to the droplet volume in order to avoid the effect of drop size.

Overall, sessile-drop method provides us with 2 contact angle values (from left side and right side of the droplet). The two are then averaged using the evaluation plugin of ImageJ program to finally report the average value of contact angle for the given surface.

4.5 Evaluation of reproducibility

To describe the reproducibility of our measurements normal distribution was chosen to determine the measurement accuracy, standard deviation and errors.

Normal probability distribution is a continuous probability distribution that describes many quantities and phenomena whose values are symmetrically clustered around a mean value to form a characteristic curve called Gaussian Curve (figure 22). This type of distribution is commonly used to represent real-valued random variables with unknown distribution. This approximation could be made thanks to the central limit theorem, which states that under certain conditions, the average value of a random variable with finite mean and variance is a random variable itself, and, with an increasing number of values, its distribution eventually converges to a normal distribution as well.

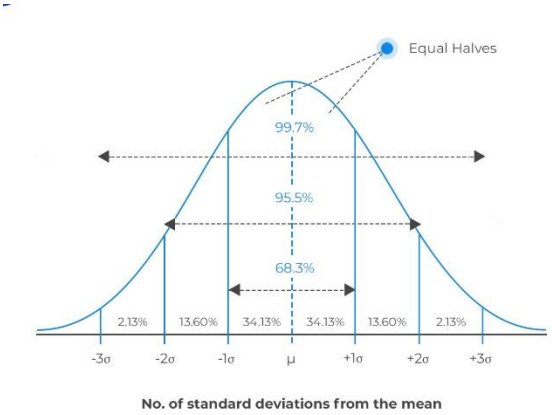

Fig. 22: Gaussian curve – normal probability distribution

For the purposes of measurements presented in this thesis, 20 singular measurements were effectuated on each type of sample. This amount of data is sufficient enough to provide trustworthy and credible results.

5 RESULTS

This chapter resumes all the outcomes of effectuated experiments along with the results of provided statistical analyze.

5.1 Relative density and grain size

Relative densities as well as the volume of open porosity of all types of samples is summarized in the table 11. This table also comprises the values of average grain size for each type of sample. The values were calculated from SEM images using the line interception method in the ImageJ software.

Tab. 11: Summary of sintering temperatures, relative densities, volume of open porosity and average grain size

Sample	*Sintering temperature [°C]*	ρ_{rel} *[%]*	V_O [%]	*Average grain size [μm]*
ZN11	*1100*	*99.5*	*0.5*	*7.45*
TI11	*1100*	*99.9*	*0.7*	*2.81*
HA11	*1100*	*75.1*	*21.1*	*0.62*
AL15	*1500*	*94.5*	*3.5*	*0.86*
AL16	*1600*	*99.0*	*0.2*	*0.94*
ZR13	*1300*	*76.4*	*22.3*	*0.13*
ZR14	*1400*	*90.5*	*4.4*	*0.18*
ZR15	*1500*	*98.8*	*0.4*	*0.32*
ZR16	*1600*	*99.3*	*0.8*	*0.55*

5.2 Surface microstructure

Samples of each type of material were analyzed in the scanning electron microscope (SEM). Photos from the SEM analysis provide very useful information abou the surfaces' microstructure and porosity. Thanks to these pictures, the relative amount of open porosity and relative densities of given samples could be correlated with sintering temperatures and average grain size values.

The microstructures of all types of samples are displayed in the figures below.

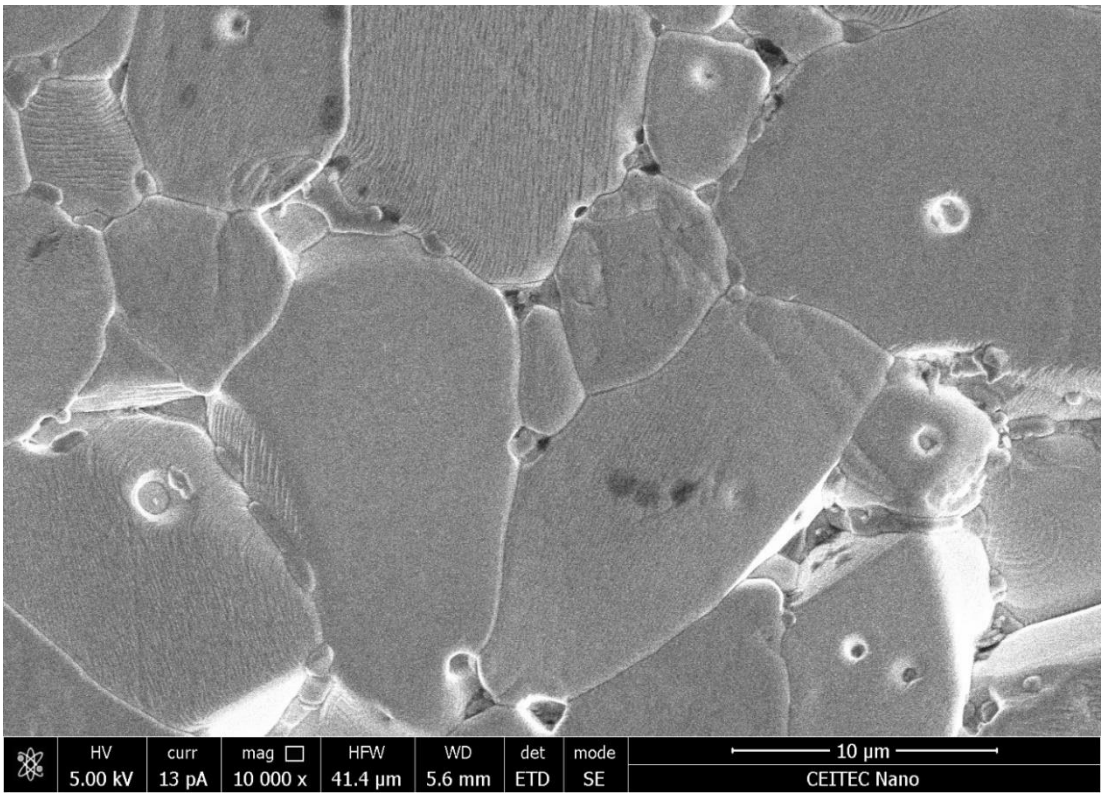

Fig. 23: Microstructure of ZN11 surface after thermal etching

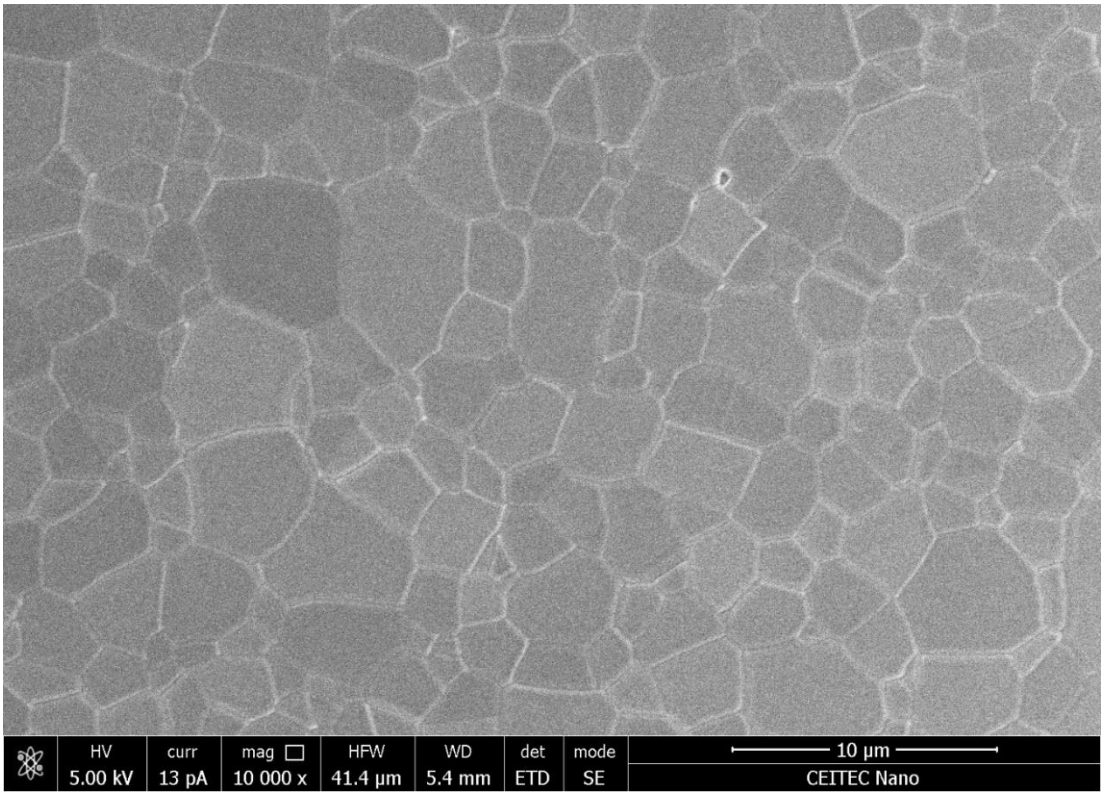

Fig. 24: Microstructure of TI11 after thermal etching

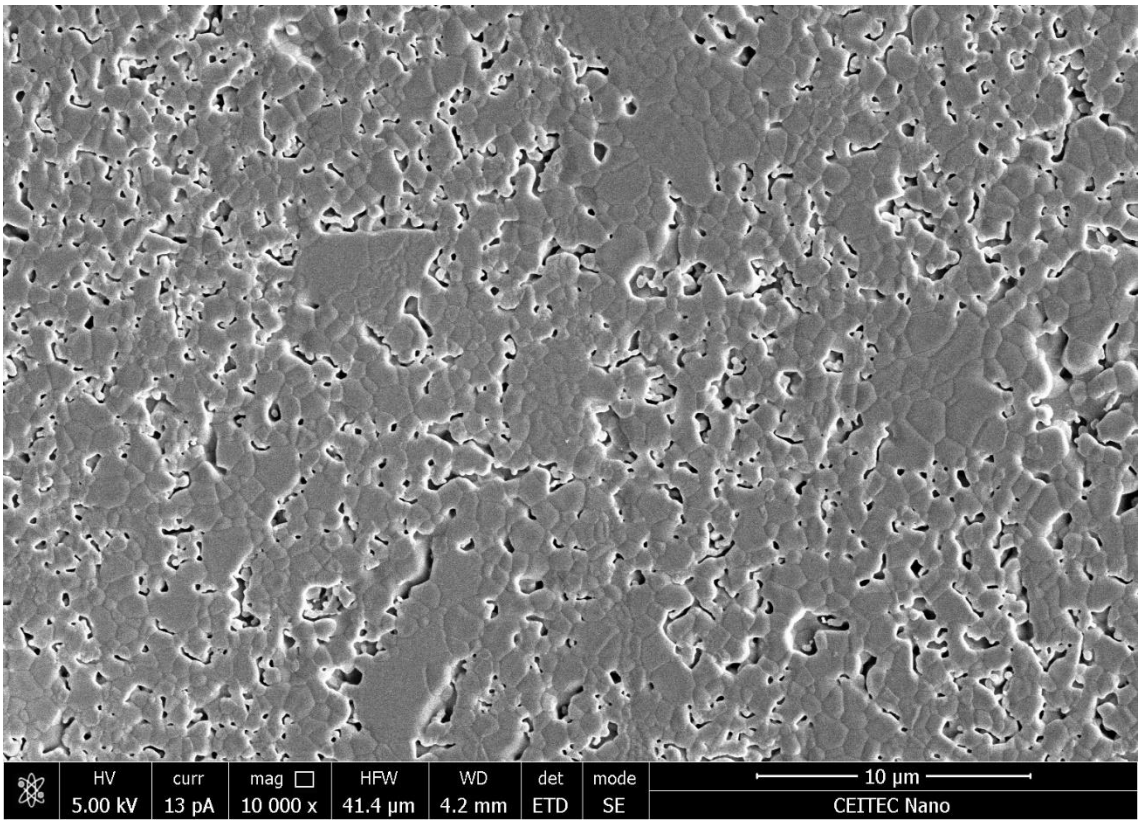

Fig. 25: Microstructure of HA11 after thermal etching at the magnification of 10000x

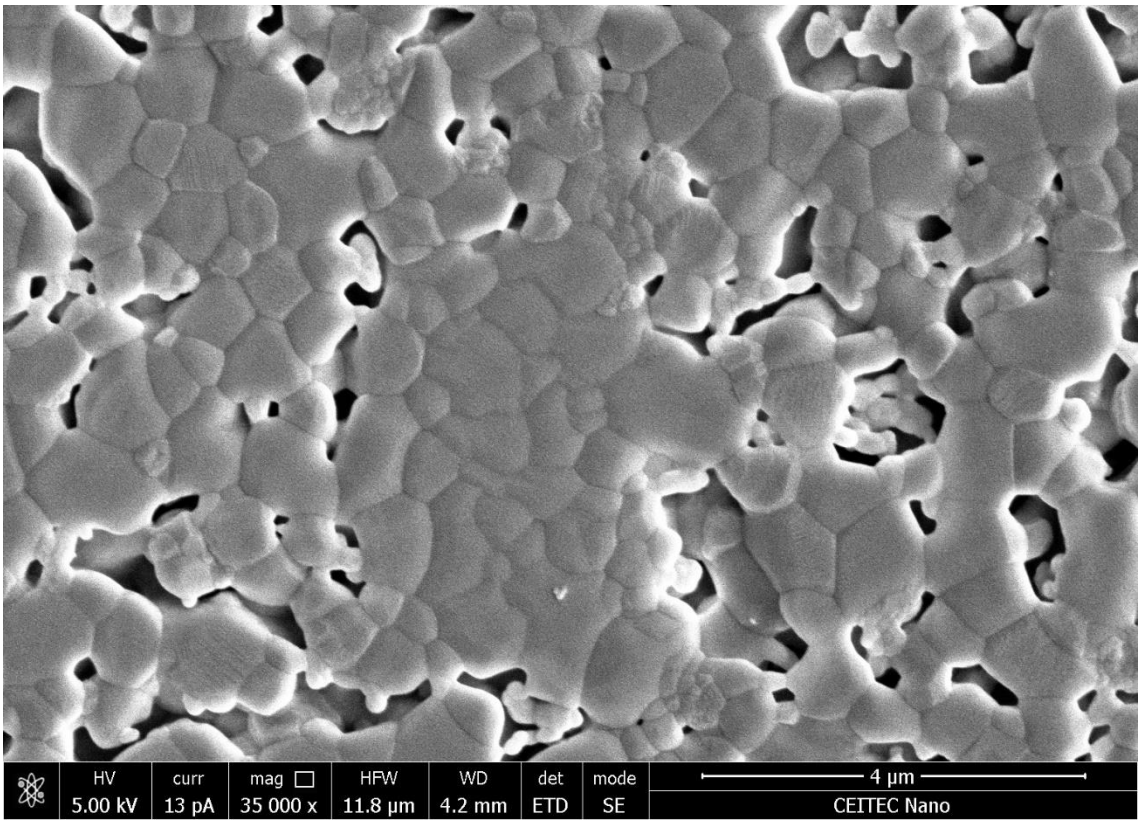

Fig. 26: Microstricture of HA11 at magnification of 35000x after thermal etching

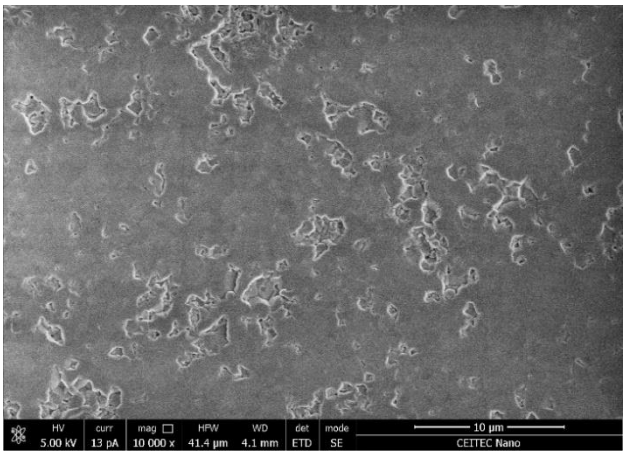

Fig. 27: Microstructure of AL15 after thermal etching

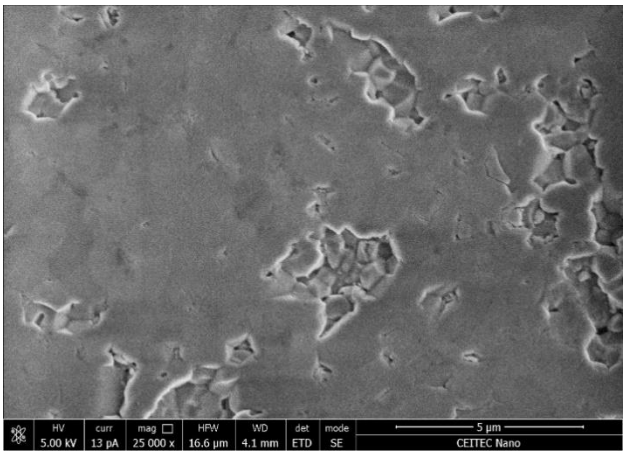

Fig. 28: Microstructure of AL16 after thermal etching

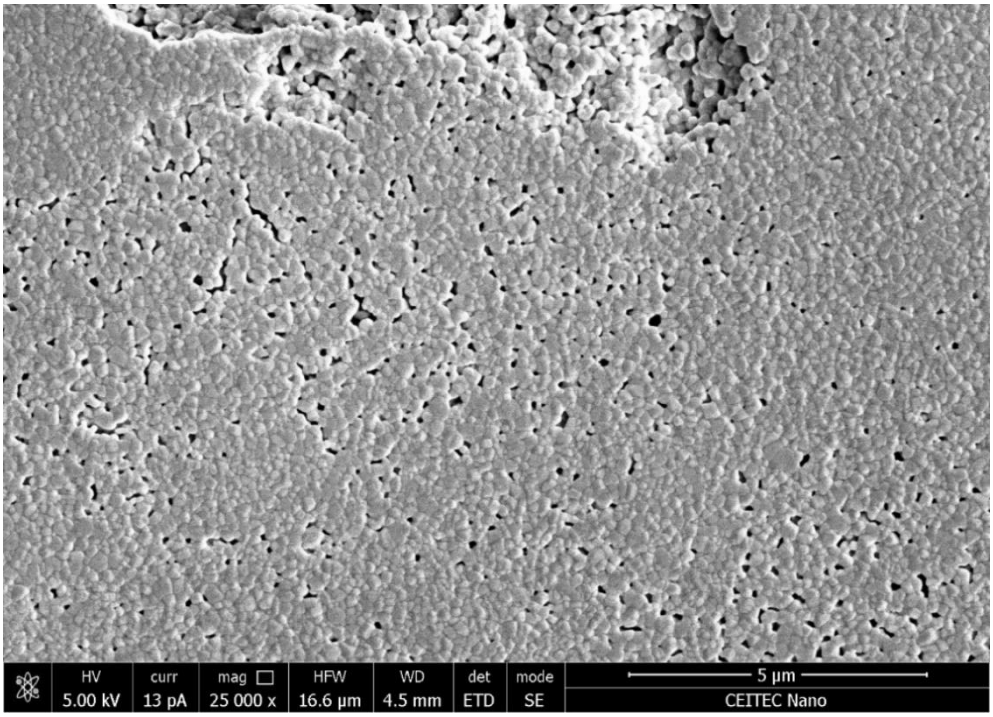

Fig. 29: Microstructure of ZR13 after thermal etching – porous structure

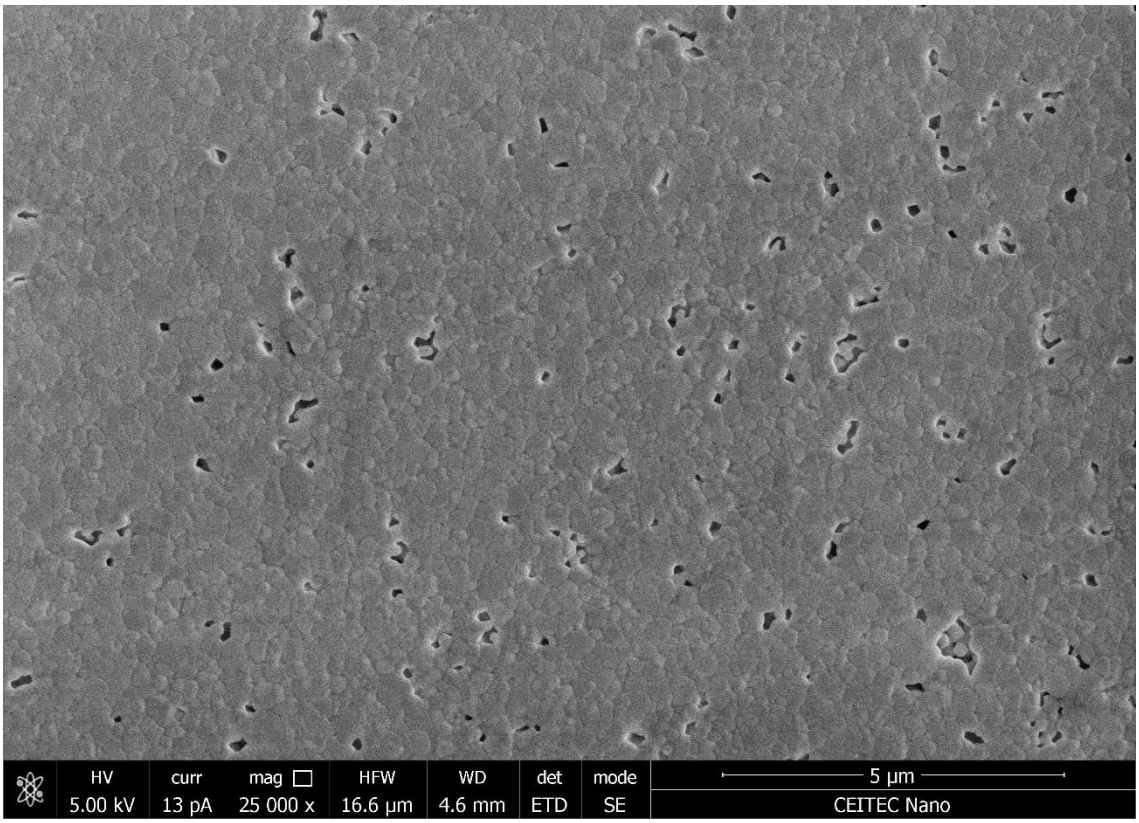

Fig. 30: Microstructure of ZR14 after thermal etching

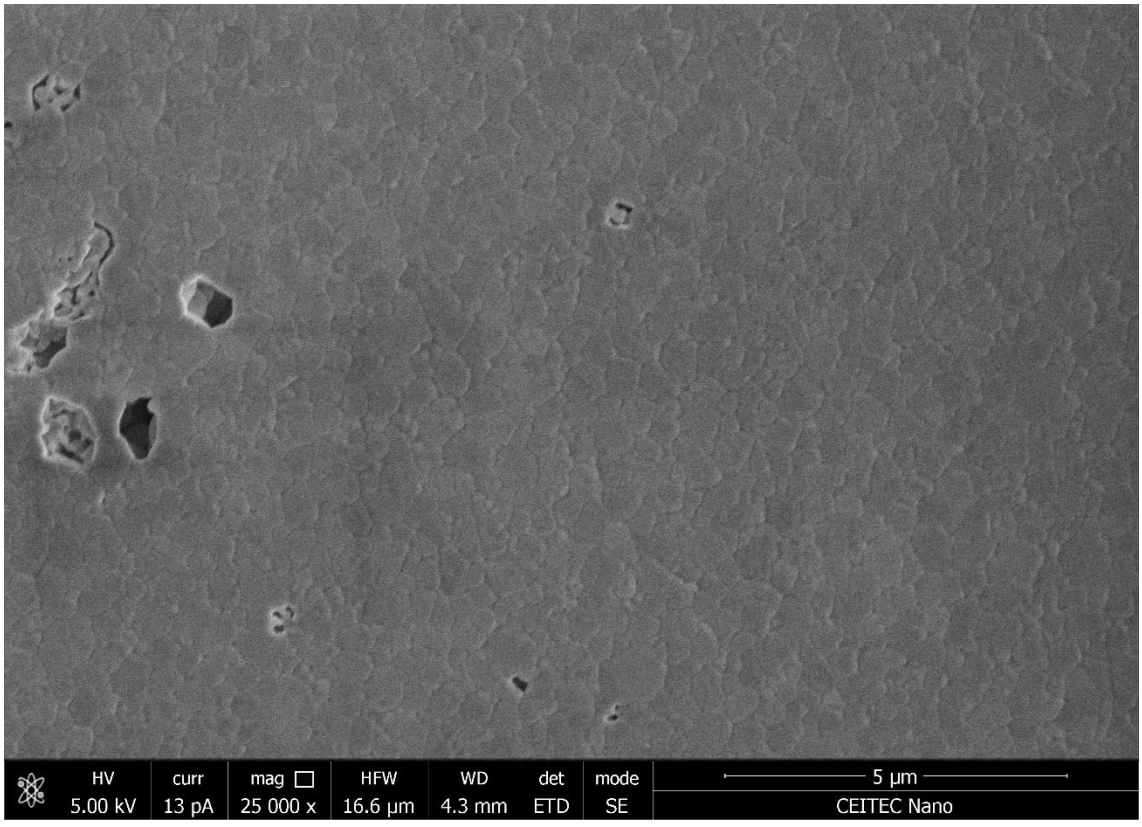

Fig. 31: Microstructure of ZR15 after thermal etching

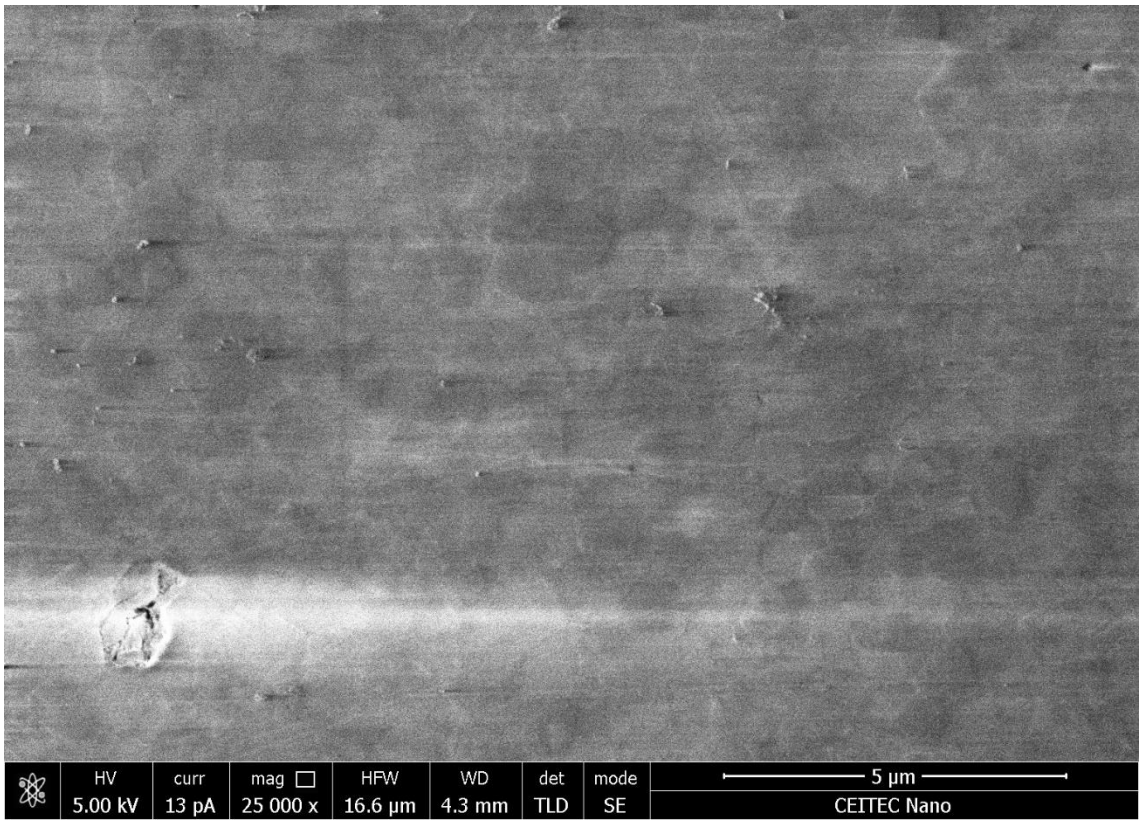

Fig. 32: Microstructure of ZR16 after thermal etching

5.3 Contact angle measurements

As stated in previous chapters, in order to assure the reproducibility of results, 20 measurements of contact angles were made for each type of sample. Values of contact angles show the convergence to the normal probability distribution. For each sample type, average contact angle value was determined within a confidence interval of 99%. All the results are summarized in the tables below. They comprise the values of average contact angles along with their standard deviation.

5.3.1 Referral measurements

Firstly, contact angles were measured on selected monocrystals of sapphire and silica. These measurements were very useful for further reference and comparison to the obtained values measured on studied ceramic materials. Figures 33 and 34 show the deposited droplets on the surfaces of sapphire and silica, respectively.

Tab. 12: Summary of measured water contact angles, of values of standard deviation and lower/upper limits of confidence intervals for reference materials

Sample	*Average contact angle [°]*	*Standard deviation*	*Confidence interval – low**	*Confidence interval – up**
Sapphire SA	*84.7*	*2.15*	*83.7*	*85.6*
Silica SI	*26.7*	*3.81*	*24.6*	*28.8*

*Confidence interval – low is the abbreviation for the lower boundary of a confidence interval

**Confidence interval – up is the abbreviation for the upper boundary of a confidence interval

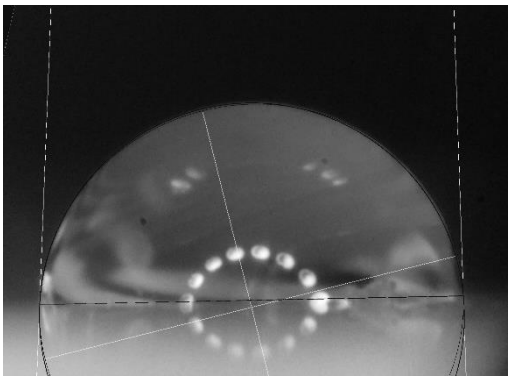

Fig. 33: WCA on sapphire surface

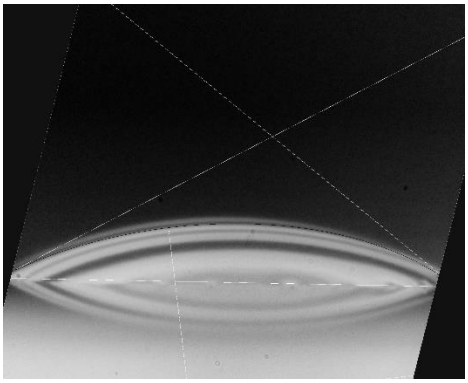

Fig. 34: WCA on silica surface

5.3.2 Contact angles on untreated surfaces

Obtained values of average contact angles for all the samples in the "control group" are stated in the Table 13. "Control group" of samples comprises all the samples whose surfaces were only polished prior to the measurements. No further surface treatment was effectuated on these surfaces. The table also contains values of standard deviation for each sample. The last two columns provide us with the lower and upper boundaries of 99% confidence interval attributed to each measurement.

Tab. 13: Summary of measured water contact angles, of values of standard deviation and lower/upper limits of confidence intervals for untreated surfaces

Sample	*Average contact angle [°]*	*Standard deviation*	*Confidence interval – low**	*Confidence interval – up**
ZN11	*68.4*	*10.4*	*62.4*	*74.4*
TI11	*67.0*	*8.98*	*60.1*	*74.0*
HA11	*61.4*	*7.0*	*55.9*	*66.8*
AL15	*73.7*	*8.26*	*68.2*	*79.2*
AL16	*78.3*	*9.87*	*71.8*	*84.9*
ZR13	*46.6*	*7.56*	*40.1*	*53.1*
ZR14	*64.9*	*8.13*	*59.7*	*70.2*
ZR15	*71.2*	*5.20*	*67.6*	*74.8*
ZR16	*82.9*	*3.64*	*80.8*	*85.0*

The evolution of contact angle on the surfaces of zirconia sintered at different temperatures are demostrated through the series of figures 35, 36, 37 and 38. Figure 39 presents an overview of determined contact angle values for all types of samples.

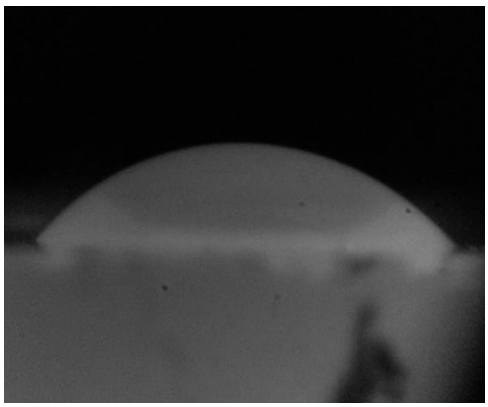

Fig. 35: WCA on the surface of ZR13

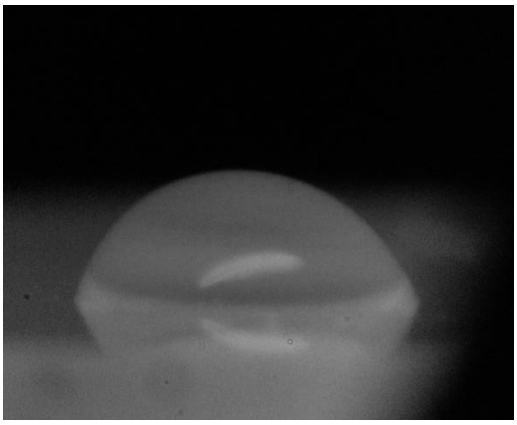

Fig. 36: WCA on the surface of ZR14

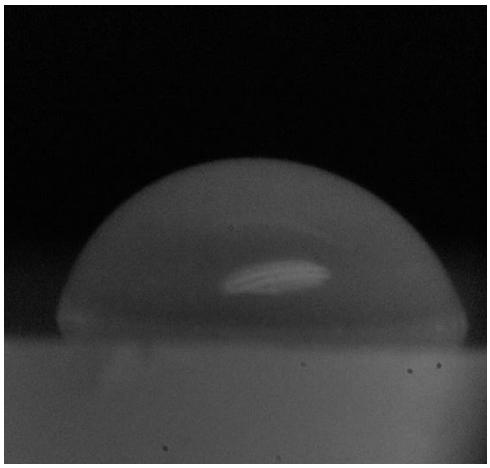

Fig. 37: WCA on the surface of ZR15

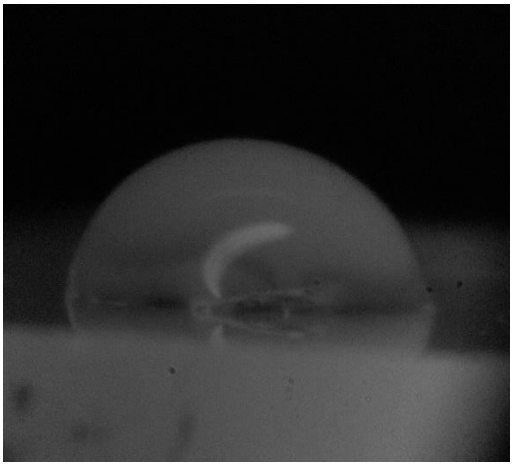

Fig. 38: WCA on the surfce of ZR16

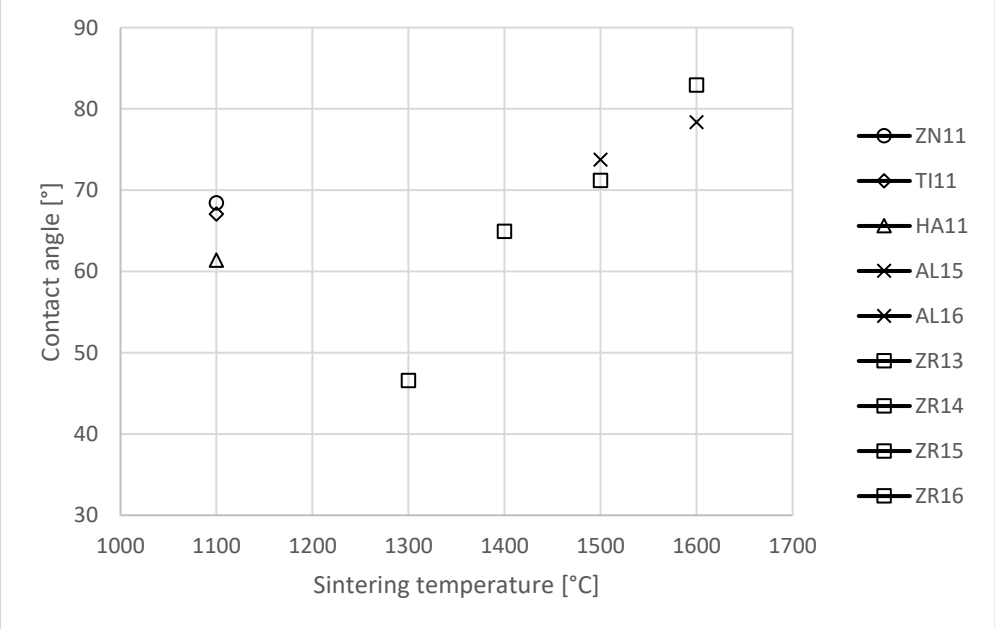

Fig. 39: Relation between contact angle values on surfaces and sintering temperatureZirconia was sintered at total at 4 different sintering temperatures, therefore

the relations between relative density, grain size and contact angles are demonstrated through the values obtained for ZR13, ZR14, ZR15 and ZR16. Figure 40 presents the dependence of relative density of zirconia as a function of its sintering temperature.

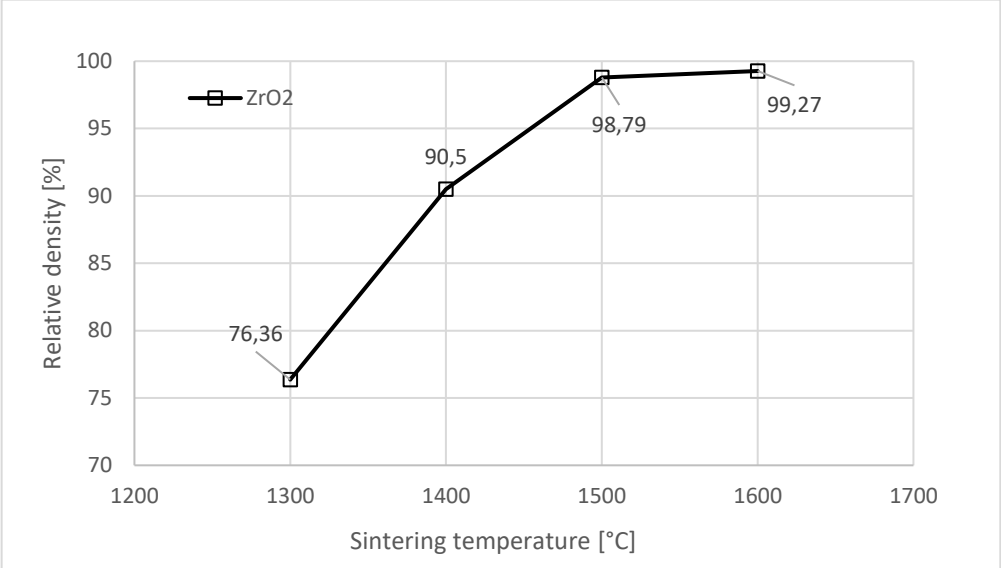

Fig. 40: Dependece of relative density and sintering temperature of Zirconia

Figure 41 demonstrates the relation between contact angle values of zirconia and its relative densities

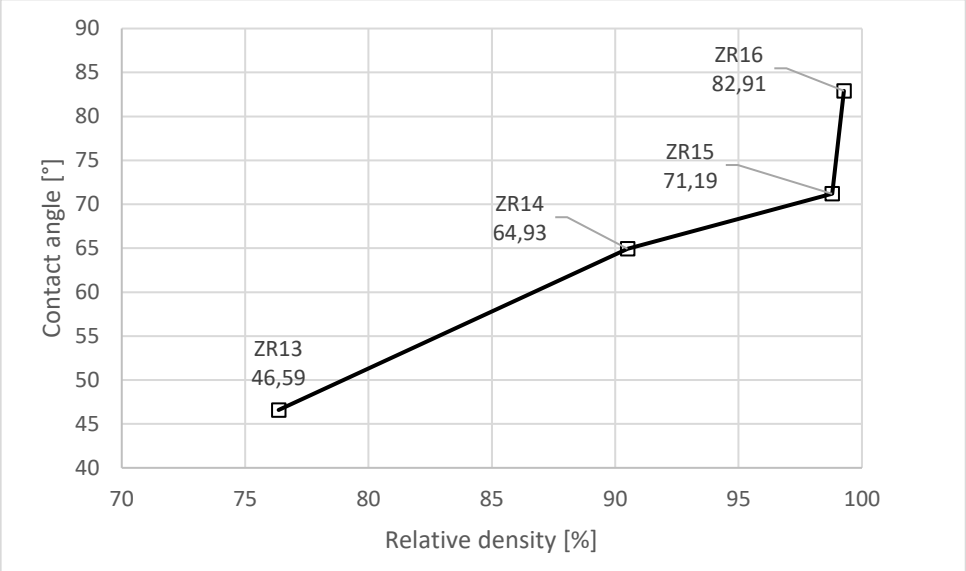

Fig. 41: Dependence of contact angle values on relative densities of Zirconia sintered at different temperatures

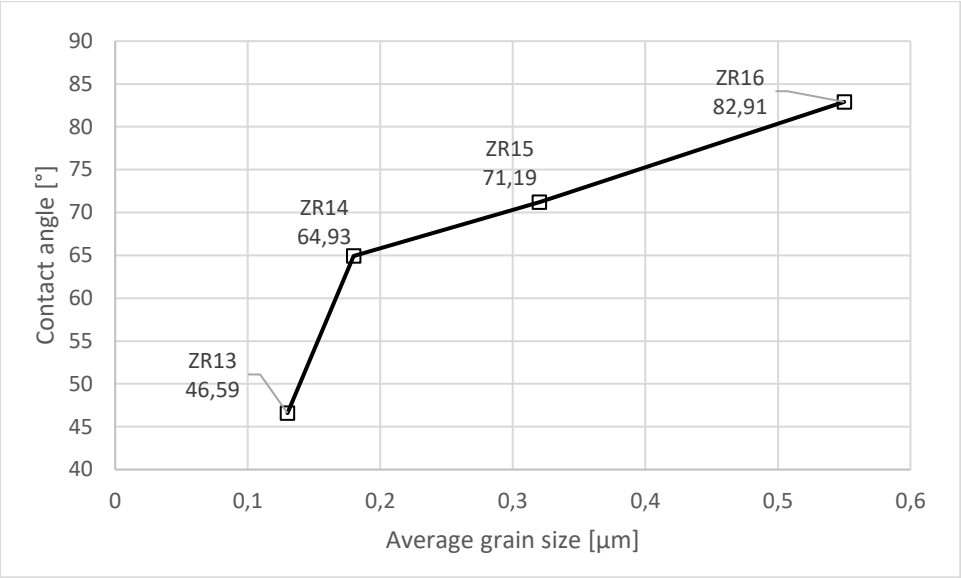

Fig. 42: Relation of contact angle values and average grain size of Zirconia sintered at different temperatures

The relation between contact angle values of zirconia and average grain size value are displayed in the figure 42.

5.3.3 Contact angles after calcination

Once the measurements on untreated surfaces were finished, the "control group" of samples together with the referral samples of sapphire and silica were put in the tube furnace for calcination. Then, samples were immersed into the deionized water to avoid contamination during their transport between laboratories. Further measurements were performed right afterwards in order to shorten the samples' exposure to the ambient air as much as possible. Results of contact angles, standard deviations and values of the boundaries of confidence intervals are given un the Table 14.

Tab. 14: Summary of measured water contact angles, standard deviations and of values of lower/upper limits of confidence intervals for calcinated samples

Samples	*Average contact angle [°]*	*Standard deviation*	*Confidence interval – low**	*Confidence interval – up**
SA-C	*32.1*	*4.19*	*29.0*	*35.2*
SI-C	-	-	-	-
ZN11-C	*24.7*	*3.22*	*22.1*	*27.3*
TI11-C	*18.0*	*4.17*	*15.1*	*20.9*
HA11-C	-	-	-	-
AL15-C	*22.4*	*4.05*	*19.6*	*25.2*
AL16-C	*26.8*	*4.99*	*23.1*	*30.5*
ZR13-C	-	-	-	-
ZR14-C	-	-	-	-
ZR15-C	*16.3*	*5.31*	*12.3*	*20.3*
ZR16-C	*35.9*	*2.14*	*33.8*	*38.1*

Compared to the values obtained during the “control” measurement, the calcinated surfaces report significantly lower water contact angles. Furthermore, the values of standard deviations are also lower, suggesting that the surfaces were more homogenous. Some values in the tables are missing because of the inability of contact angle evaluation. Droplets of water deposited on the calcinated surface spread across the whole surface almost immediately and evaporated before the photo was taken.

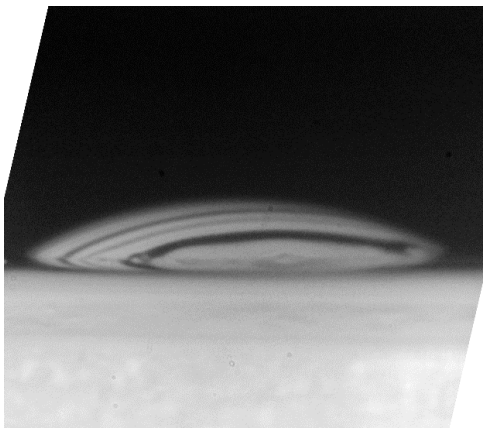

Fig. 43: WCA on Zr15 after calcination

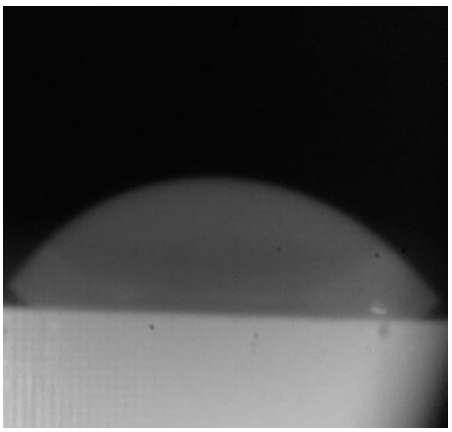

Fig. 44: WCA on ZR16 after calcination

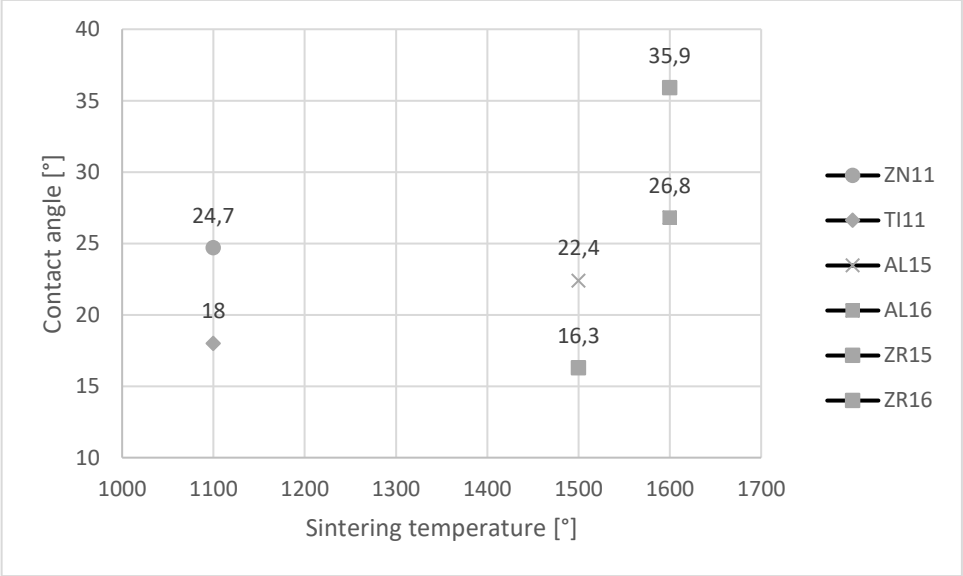

Fig. 45: Overview of contact angle values of all sample types with respect to the sintering temperature

Summarized results from contact angle measurements on the calcinated samples are shown in the figure 45.

5.3.4 Contact angles on surfaces cleaned with ethanol

Contact angle measurements on calcinated samples were performed with intention of shortening their exposure to the ambient air as much as possible. Right after the measurements, the samples were immersed into the ethanol for at least two hours. Then,

they were pulled out and left to dry in the ambient air. Table 15 shows obtained results of contact angles, standard deviation and values of confidence intervals boundaries on surfaces cleaned with ethanol.

Tab. 15: Summary of measured water contact angles, standard deviations and of values of lower/upper limits of confidence intervals for surfaces cleaned with ethanol

Sample	*Average contact angle [°]*	*Standard deviation*	*Confidence interval – low*	*Confidence interval – up*
SA-CE	*45.7*	*3.44*	*43.5*	*47.9*
SI-CE	-	-	-	-
ZN11-CE	*47.1*	*2.76*	*44.9*	*49.3*
TI11-CE	*52.4*	*4.15*	*48.7*	*56.1*
HA11-CE	-	-	-	-
AL15-CE	*44*	*3.75*	*49.5*	*55.3*
AL16-CE	*47.4*	*4.11*	*43.8*	*51.0*
ZR13-CE	*21.7*	*4.98*	*18.0*	*25.4*
ZR14-CE	*25.8*	*4.66*	*22.6*	*29.1*
ZR15-CE	*53.6*	*2.14*	*51.5*	*55.7*
ZR16-CE	*60.8*	*2.87*	*58.1*	*63.5*

Similarly to the previous measurement on calcinated surfaces, some of the values in the table are missing. These values were impossible to determine and to evaluate, because the spreading of water droplet across the surface was very significant. All the gained results are displayed in the figure 46, which illustrates the values of contact angles of all sample types as a function of sintering temperatures.

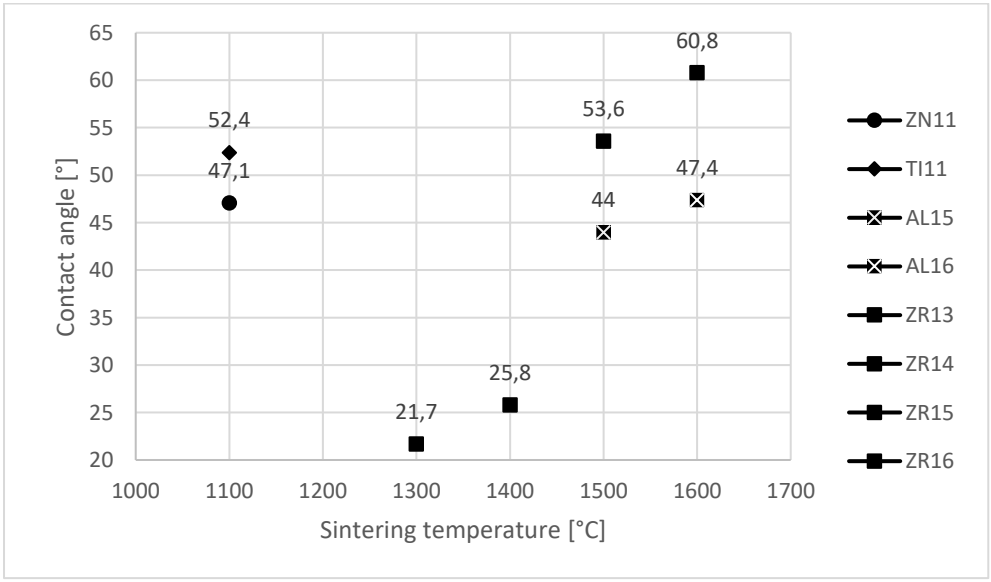

Fig. 46: Overview of contact angle values on the surfaces cleaned with ethanol with respect to the sintering temperature

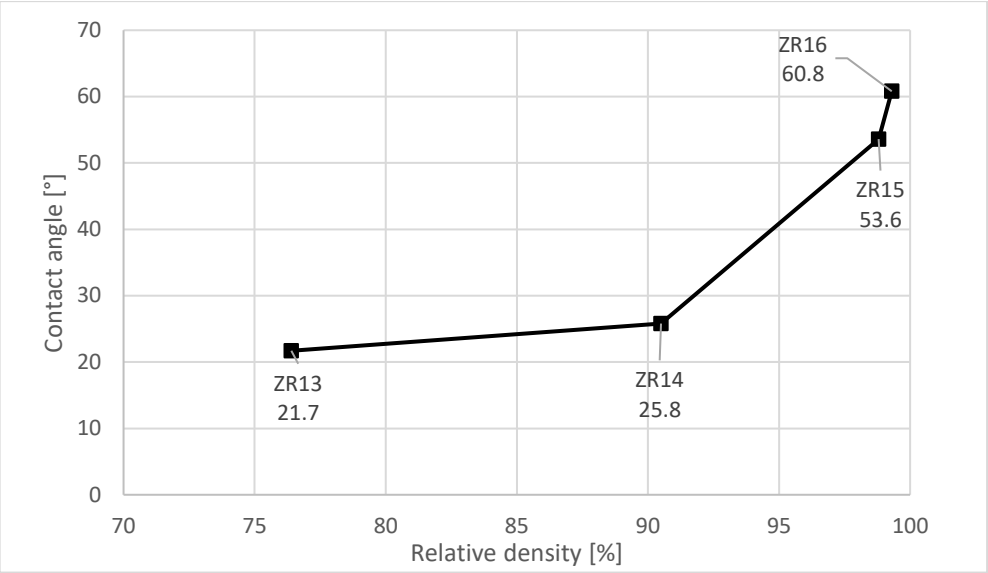

Fig. 47: Dependence of contact angle values and relative density of Zirconia sintered at different temperatures

Values of contact angles for zirconia sintered at various temperatures as a function of its relative densities are shown in the figure 47 above.

Results of the measurements presented above are discussed and explained in the following section. Changes of WCA values after different surface treatments is also explored in the discussion. The ongoing part describes the changes of contact angle values as a consequence of adsorption of volatile organic compounds to the surfaces.

6 DISCUSSION

In common environments, the presence of adsorbed organic compounds on the surface of inorganic materials is unavoidable. Contamination of surfaces is mostly adventitious and unfavorable – it may influence the functionality and performance of semiconductors, or cause a lowering of the work function of electrically conductive oxides. Furthermore, the presence of organic compounds has an impact to the adhesion properties of surfaces – the efficiency of surface modifications may be lowered. [10], [33], [35]

Sources and nature of adsorbed organic compounds may be various – contamination may come from the sample preparation, from industrial processing or from the environment itself. Volatile organic compounds present in the ambient air may originate from both anthropogenic and biogenic sources. Their chemical nature as well as their abundance in specific environments often depends on their particular source. It is at utmost importance to assess the circumstances of their adsorption as well as the changes they cause to the surfaces of materials.

It has been reported that the presence of volatile organic compounds on the surface of an inorganic material results in decrease of its hydrophilic character. To assess the pre-assumed contamination of a surface, contact angle measurement seems to be the most convenient and the most credible method to determine surface energy and wettability of surface and thus describe changes caused by adsorbed contaminants.

Ceramic oxides, such as alumina, zirconia and titanium dioxide, hydroxyapatite and zinc oxide were selected to undertake measurements effectuated on their surfaces. The value of surface energy is characterized by contact angle values. The higher the values of angles are, the higher is the energy of a given surface. [10], [36]

Observed changes in surface characteristics after various surface treatments are discussed in following subchapters. Further observations made during the experiment, such as other factors influencing contact angle values, are also discussed in next subchapters.

6.1 Reproducibility of results

Water contact angle measurement is one of the most demonstrable methods for surface energy evaluation. Literature usually reports values of static contact angles. Although, those may not be reproducible as the conditions of measurement are usually rather dynamic – tilted surface deforms the geometry of the deposited droplet, thus it would be appropriate to distinguish two different contact angles: advancing and receding contact angle. However, during our experiment, the conditions were very stable, with no tilted surfaces nor any other dynamic elements. Therefore, this thesis always reports values of static contact angles with the accuracy and confidence listed in tables in the part “Results”.

Sessile-drop method is the simplest, yet the most convenient one for static or dynamic contact angle determination.

Statistic evaluation of every single measurement was provided in order to ensure that all the results are reproducible and relevant. Measured values corresponded to the normal distribution of random variables. Confidential intervals with confidence level of 99% were used to determine the range of values of contact angles for every ceramic material sintered at a given temperature.

6.2 Relative density and microstructure analysis

In order to report the relative porosity (or density) of each sample, density measurements were performed following Archimedes method. According to the results, HA11 and ZR13 showed values lower than 80%, which had a significant impact to the results of contact angle measurements. All of the results are supported by SEM images of microstructure.

Relative density (porosity) showed to have a very significant impact to the measurements of contact angles. Porous structures all had a common trait when it came to the determination of WCA – the deposited droplet of water spread across the whole surface and tend to infiltrate into the pores and thus evaporate very quickly. This phenomenon was manifested significantly on the calcinated surfaces of chemically cleaned surfaces.

When it comes to the microstructure itself, the relations between average grain size, relative density and sintering temperatures were well demonstrated by the example of zirconia sintered at four different temperatures. The gradual increase of sintering temperature from 1300°C to 1600°C contributed to the densification of the structure and reduction of open porosity in the bulk material. With rising sintering temperature, the growth of grains was observed at the same time. The dependence of relative density and the value of contact angle is discussed in the part “Contact angle measurements”.

6.3 Contact angle measurements

Surface energy of a particular material is a result of many contributing factors, such as roughness, heterogeneity, crystal structure, chemical bonding and many others. It is apparent that each material has its own surface characteristics – degree of wetting, hydrophilic or hydrophobic character, higher or lower surface energy etc. However, due to the presence of volatile organic compounds in the environment, surfaces of inorganic materials, such as metallic oxides, are contaminated by adsorbed organic compounds. The adsorption of organic substances may change the surface characteristics to such an extent that its functionality or modification/treatment susceptibility is lowered. First measurements of contact angles on the surfaces of oxide ceramics were performed in normal laboratory conditions, when the examined surfaces were exposed to the ambient air of the laboratory for at least 3 consecutive days.

Results obtained from these measurements (summarized in the table 12) are further referred to as “referral measurements” – they were not subject to any thermal or chemical treatment.

The values are highly specific for different materials, as shown on Fig 39. Furthermore, there are also differences within the samples of alumina and zirconia sintered at different temperatures. After density measurements and SEM analysis of microstructure, these

differences were attributed to the diversity of relative densities originating from four different sintering temperatures.

Next measurements were performed after the thermal process of calcination. This procedure was chosen to assess the differences in contact angle values before and after thermal "cleaning" of the surface. Assuming that untreated surfaces of ceramic oxides are contaminated by adsorbed volatile organic compounds, this procedure was thought to remove the adsorbed contaminants to provide values of contact angles on clean surfaces.

Further measurements with the calcinated samples were performed after their cleaning in ethanol. Before their immersion into ethanol, samples were exposed to the ambient air for approximately an hour.

Table 16 compares the results of WCA obtained on untreated surfaces, on calcinated surfaces and on surfaces cleaned with ethanol

Tab. 16: Summary of contact angle values on untreated surfaces and on surfaces after thermal and chemical treatment

Sample type	*Average contact angle on untreated surface [°]*	*Average contact angle after calcination [°]*	*Average contact angle after ethanol treatment [°]*
SA	*84.7*	*32.1*	*45.7*
SI	*26.7*	-	-
ZN11	*68.4*	*24.7*	*47.1*
TI11	*67.0*	*18.0*	*52.4*
HA11	*61.4*	-	-
AL15	*73.7*	*22.4*	*44*
AL16	*78.3*	*26.8*	*47.4*
ZR13	*46.6*	-	*21.7*
ZR14	*64.9*	-	*25.8*
ZR15	*71.2*	*16.3*	*53.6*
ZR16	*82.9*	*35.9*	*60.8*

Values of WCA decreased significantly after the calcination process. Some of the values were not determined because the droplet of water evaporated right after the deposition due to its immediate spread across the surface.
The trend of decreasing value of contact angle is observed on the referral samples of silica and sapphire, as well.

Calcination process removed the contaminating organic compounds adsorbed on the surface. Generally, the differences in WCA values between untreated and calcinated surfaces were as high as 40-50°. Values of contact angles on clean surfaces are though relevant for the assessment of materials' hydrophilicity, adhesivity and surface energy. The exposure of samples to the surrounding air resulting in the increase of WCA values is an unambiguous proof of adventitious surface contamination.

Another surface treatment performed with intention to clean the surface and remove contaminating organic compounds was of a chemical origin. After being exposed to the

ambient air for approximately an hour, the samples were immersed into the ethanol for another 2 hours and then pulled out to be left to dry in the surrounding air. It is important to note that the drying process was not longer than 2 minutes long due to the fast evaporation of ethanol. Results of measured contact angles show a little decrease in the values compared to the results of untreated surfaces, yet the values are not as low as the values right after calcination. This difference may have a simple reason: before the samples were immersed into the ethanol, they were exposed to the laboratory environment for a relatively sufficient period of time to adsorb some organic compounds on their surfaces. Moreover, cleaning the surface with ethanol cannot surpass the effect of calcination, which, according to the results, successfully removed contaminating adsorbents from the surfaces.

Fig. 48 comprises all the values of contact angles measured on all type of samples with untreated surfaces, calcinated surfaces and surfaces cleaned with ethanol.

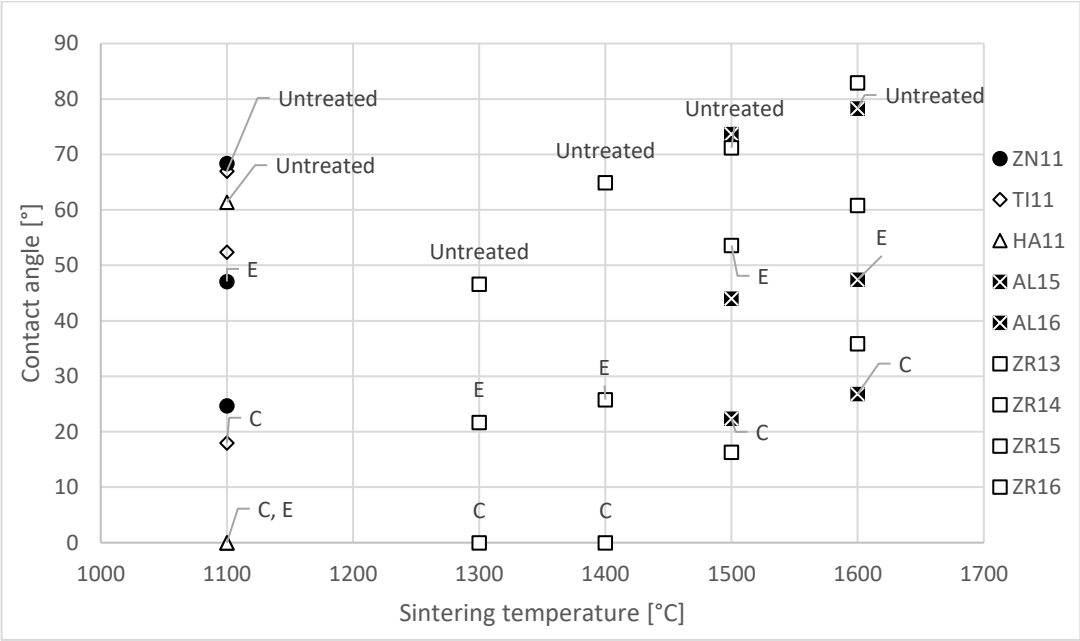

Fig. 48: Summary of contact angles on all types of samples for untreated surfaces, calcinated surfaces (C) and surfaces cleaned with ethanol (E)

Relations between contact angle values, relative densities, grain size and sintering temperatures for zirconia all together with information about the surface treatment are displayed in the graphs below. The effect of surface treatments on the surface characteristics is visible through the values of contact angles. Their differences within particular treatments indicate the presence or the absence of adsorbed contaminant on the surfaces. Moreover, sintering at four different temperatures and subsequent measurement of WCAs also revealed how surface characteristics change with increasing density and grain size. All these effects are presented and displayed in the figures 49 and 50 below.

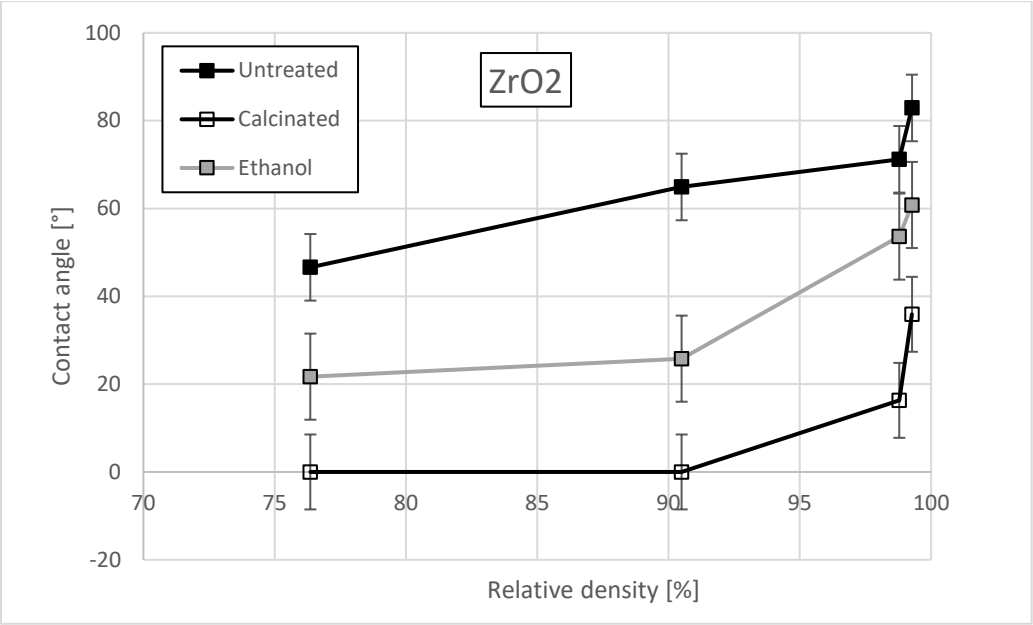

Fig. 49: Dependence of contact angles of zirconia on relative density for different surface treatments

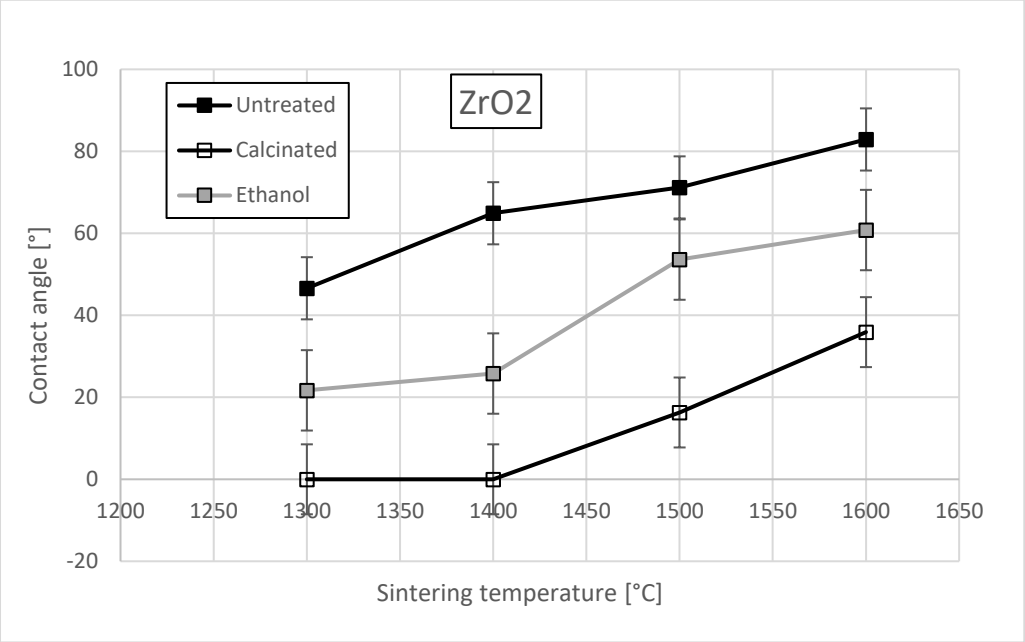

Fig. 50: Dependence of contact angles of zirconia on sintering temperature for different surface treatments

7 CONCLUSIONS

This research was focused on the evaluation and analyze of changes on surfaces of ceramic oxides caused by adsorption of organic molecules. Characterization of surface was provided by contact angle measurements using sessile-drop technique. This technique provided reproducible and valuable data that consisted of static contact angle values. Thanks to the water contact angle measurements, the changes in surface tension, wettability and adhesivity were directly assessed.

According to the resources, the contamination of surface in ambient air is unavoidable. Organic compounds are usually adsorbed on the surfaces of inorganic materials, such as oxide ceramics studied in this work. The contamination from volatile organic gases may originate from both anthropogenic and biogenic sources. The abundance of particular compounds in the surrounding atmosphere depends on their source as well as on the environment they were emitted into. Different sources are responsible for emissions of many chemical species with different average lifetimes in the atmosphere and with various reactivity.

Monitoring and detecting organic contamination on inorganic surfaces has been done using many methods including ToF-SIMS, Raman spectroscopy, isotope labelling XPS (X-ray photoelectron spectroscopy) and others, the last being claimed to be the most suitable one. This experiment described the changes on surfaces caused by organic contamination through the water contact angle measurements.

After performing measurements of WCAs on samples exposed to the ambient air with no further surface treatment, other measurements were effectuated on the calcinated samples and on the surfaces cleaned with ethanol. Results from all measurements were compared and discussed with following findings and conclusions:

- Water contact angle measurements represent a suitable and credible way of monitoring surface changes through the changes in angle values
- The changes in WCA values between differently treated surfaces indicate the presence of contaminating compounds on the surfaces
- Presence of adsorbed organic compounds on inorganic surfaces was manifested by the increase of contact angle values
- The increase of WCA values was observed with every sample type including the referral samples of sapphire and silica
- Thermal treatment of calcination had more profound impact on the surfaces than chemical treatment in ethanol
- WCA measurements also described the changes of surface characteristics depending on the relative density and average grain size. Increasing sintering temperatures resulted in densification and grain growth which was manifested by increasing values of WCA within the zirconia samples.
- The amount of open porosity significantly changes the WCA values, because the deposited droplets immediately penetrate into the pores and subsequently evaporate

Monitoring and assessment of different contact angle values throughout the experiments lead to a following conclusion: changes on inorganic surfaces of ceramic oxides caused by the adsorption of adventitious organic compounds can be assessed and determined by contact angle measurements. Their change directly indicates the presence or absence of contaminating layer. Volatile organic compounds adsorbed from the surrounding air profoundly affect hydrophilicity, adhesivity and surface energy of inorganic surfaces. Specifically, they demonstrably increase of WCA values. Lower values of WCA are may be obtained after specific surface treatments that, by their principle, cause the removal of adsorbed compounds.

8 LITERATURE

[1] BARSOUM, Michael W. Fundamentals of ceramics. [2nd. ed.]. New York,c2003. ISBN 07-503-0902-4.

[2] ASKELAND, D.R., F. HADDLETON, P. GREEN a H. ROBERTSON. *Thescience and engineering of materials*. 7th edition. Cengage, 2015. ISBN 9781305077102.

[3] MUNZ, Dietrich a Theo FETT. *Ceramics: Mechanical Properties, Failure Behaviour, Materials Selection*. 1. Springer-Verlag Berlin Heidelberg, 1999. ISBN 978-3-642-58407-7.

[4] BERRY CARTER, C. a M. GRANT NORTON. *Ceramic materials: Science and engineering*. Second edition. New York, NY: Springer, New York, NY, 2013. ISBN 978-1-4614-3522-8.

[5] RICHERSON, David W. *Modern Ceramic Engineering: Properties, Processing, and Use Design*. 2 ed. New York: Marcel Dekker, 1992. ISBN 08-247-8634-3.

[6] PAMPUCH, Roman. *An introduction to ceramics*. 1. Springer International Publishing, 2014. ISBN 978-3-319-10410-2.

[7] FIALA, Jaroslav a Ivo KRAUS. *Povrchy a rozhraní*. 2. vydání. Praha: Nakladatelství ČVUT, 2017. ISBN 978-80-01-05881-7.

[8] Advaces in Colloid and Interface Science: *Review of non-reactive and reactive wetting of liquids on surfaces*. 2007. 2007.

[9] BERNARDIN, J.D., I. MUDAWAR, C.B. WALSH a E.I. FRANSES. Contact angle temperature dependance for water droplets on practical aluminum surfaces. In: *International Journal of Heat and Mass Transfer*. 1997, s. 1017-1033

[10] LANDOULSI, Jessem, Michel J. GENET a Yetioman TOURÉ. Organic adlayer on inorganic materials: XPS analysis selectivity tocope with adventitious contamination. *Applied Surface Science* [online]. 2016, **2016**(383), 71-83 [cit. 2020-06-25]. DOI: https://doi.org/10.1016/j.apsusc.2016.04.147. Dostupné z: https://www.sciencedirect.com/science/article/abs/pii/S0169433216309357

[11] KOHLI, Rajiv a K.L. MITTAL. *Developments in Surface Contamination and Cleaning: Fundamentals and Applied Aspects*. William Andrew, 2008. ISBN 9780815515555.

[12] RAHAMAN, Mohammed. *Sintering of Ceramics*. CRC Press, 2007. ISBN 9780849372865.

[13] Oxidová keramika. In: *Vscht.cz* [online]. Praha [cit. 2020-06-25]. Dostupné z: http://old.vscht.cz/sil/keramika/Ceramic_Technology/SM-Lect-8-C.pdf

[14] OVČAČÍKOVÁ, Hana a Jozef VLČEK. SPECIÁLNÍ KERAMICKÉ MATERIÁLY. In: *Fmmi.vsb.cz* [online]. Ostrava, 2013 [cit. 2020-06-25]. Dostupné z: https://www.fmmi.vsb.cz/export/sites/fmmi/modin/cs/studijni-opory/resitelsky-tym-2-metalurgie/specialni-keramicke-materialy/Ovcacikova_Specialni-keramicke-materialy.pdf

[15] POULOMI, Roy, Steffen BERGER a Patrik SCHMUKI. TiO2 Nanotubes: Synthesis and Applications. *A Journal of the German Chemical Society* [online]. 2011, **2011** [cit. 2020-06-25]. DOI: 10.1002/anie.201001374. Dostupné z: https://onlinelibrary.wiley.com/doi/full/10.1002/anie.201001374

[16] LORYUENYONG, Vorrada et al. Sol-gel derived mesoporous titania nanoparticles: Effects of calcination temperature and alcoholic solvent on the photocatalytic behavior. *Ceramics International* [online]. 2012, **2012**(3), 2233-2237 [cit. 2020-06-25]. DOI: 10.1016/j.ceramint.2011.10.072. Dostupné z: https://www.sciencedirect.com/science/article/pii/S0272884211009278

[17] LÓPEZ, V.H. a A.R. KENNEDY. Flux-assisted wetting and spreading of Al on TiC. *Journal of Colloid and Interface Science*. 2006, **298**(1), 356-362. DOI: 10.1016/j.jcis.2005.12.040. ISSN 00219797. Dostupné také z: https://linkinghub.elsevier.com/retrieve/pii/S0021979705012877

[18] VIANCO, P.T., F.M. HOSKING a D.R. FREAR. *Lead-Free Solders for Electronics Applications: Wetting Analysis*. Albuquerque: Sandia National Laboratories, 1991.

[19] MARMUR, Abraham. Thermodynamic aspects of contact angle hysteresis. *Advances in Colloid and Interface Science*. 1994, **1994**(50), 121-141. DOI: 10.1016/0001-8686(94)80028-6.

[20] WOLANSKY, Gershon a Abraham MARMUR. Apparent contact angles on rough surfaces: the Wenzel equation revisited. In: *Colloids and Surfaces A: Physicochemical and Engineering Aspects*. 1999, s. 381-388. DOI: 10.1016/S0927-7757(99)00098-9.

[21] KUMAR, Girish a K. Narayan PRABHU. Review of non-reactive and reactive wetting of liquids on surfaces. *Advances in Colloid and Interface Science*. **2007**, 61-89. DOI: 10.1016/j.cis.2007.04.009.

[22] ADAMSON, Arthur W. a Alice P. GAST. *Physical Chemistry of Surfaces*. 6th edition. 1997. ISBN 978-0-471-14873-9.

[23] EUSTATHOPOULOS, N. Dynamics of wetting in reactive metal/ ceramic systems. *Acta Materialia*. 1998, **1998**(7), 2319-2327. DOI: 10.1016/S1359-6454(98)80013-X.

[24] MORRA, M., E. OCCHIELLO a F. GARBASSI. Knowledge about polymer surfaces from contact angle measurements. *Advances in Colloid and Interface Science*. 1990, **1990**(1), 79-116. DOI: 10.1016/0001-8686(90)80012-O.

[25] KANDLIKAR, Satish G. a Mark E. STEINKE. Contact angles and interface behavior during rapid evaporation of liquid on a heated surface. *International Journal of Heat and Mass Transfer*. 2002, **2002**(18), 3771-3780. DOI: doi.org/10.1016/S0017-9310(02)00090-X.

[26] KALIN, M. a M. POLAJNAR. The wetting of steel, DLC coatings, ceramics and polymers with oils and water: The importance and correlations of surface energy, surface tension, contact angle and spreading. *Applied Surface Science*. **2014**, 97-108. DOI: 10.1016/j.apsusc.2013.12.109.

[27] HUHTAMÄKI, T., X. TIAN a J.T. et al KORHONEN. Surface-wetting characterization using contact-angle measurements. *Nature*. 2018, **2018**(13), 1521–1538. DOI: 10.1038/s41596-018-0003-z.

[28] PHARK, Jin-Ho, Sillas Jr DUARTE, Harold KAHN, Markus B. BLATZ a Avishai SADAN. Influence of Contamination and Cleaning on Bond Strength to Modified Zirconia. *National Library of Medicine*. **2009**(12), 1541-1550. DOI: 10.1016/j.dental.2009.07.007.

[29] WATTS, J.F. Microbeam analysis applied to adhesion, surfaces and interfaces. *Microchimica Acta*. 2009, **2009**(164), 379–385. DOI: 10.1007/s00604-008-0070-x.

[30] DÍAZ, Eva, Salvador ORDÓNEZ, Aurelio VEGA a José COCA. Adsorption characterisation of different volatile organic compounds over alumina, zeolites and activated carbon using inverse gas chromatography. *Journal of Chromatography A*. 2004, **2004**(1-2), 139-146. DOI: 10.1016/j.chroma.2004.07.061.

[31] KOPPMANN, Ralf. *Volatile organic compounds in the atmosphere*. Wiley-Blackwell, 2007. ISBN 978-1-405-13115-5.

[32] *Hamiltoncompany.com: Hamilton syringes* [online]. 2020 [cit. 2020-06-26]. Dostupné z: https://www.hamiltoncompany.com/laboratory-products/syringes/general-syringes/microliter-syringes/700-series

[33] WHITCHER, Thomas a Prayoon SONGSIRIRITTHIGUL. The effect of carbon contamination and argon ion sputtering on the work function of chlorinated indium tin oxide. *Current Applied Physics*. 2014, **2014**(14(3), 472-475. DOI: 10.1016/j.cap.2014.01.003.

[34] SCHOENFISCH, Mark H., Azalia M. ROSS a Jeanne E. PEMBERTON. Electrochemical cleaning of surface-confined carbon contamination in self-assembled monolayers on polycrystalline Ag and Au. *Chemistry and Biochemistry*. 2000, **2000**(6), 2907-2914. DOI: 10.1021/la9900627.

[35] SHOENFISCH, M.H., A.M. ROSS a J.E. PEMBERTON. Electrochemical cleaning ofsurface-confined carbon contamination in self-assembled monolayers onpolycrystalline Ag and Au. Langmuir, 2000, **2000**(16), 2907–2914.

[36] BIRCH, W., A. Carré, K.L. Mittal, Wettability techniques to monitor thecleanliness of surfaces, in: R. Kohli, K.L. Mittal (Eds.), Developments in SurfaceContamination and Cleaning, William Andrew, Norwich, NY, USA, 2008, pp.693–723

[37] Materials-Alumina. *Materialsproject.org* [online]. [cit. 2020-06-26]. Dostupné z: https://materialsproject.org/materials/mp-1143/

[38] Zirconia. *Science Direct* [online]. [cit. 2020-06-26]. Dostupné z: https://www.sciencedirect.com/topics/materials-science/zirconia

[39] Alumina. *Pubchem* [online]. [cit. 2020-06-26]. Dostupné z: https://pubchem.ncbi.nlm.nih.gov/compound/Alumina

[40] Calcium Hydroxyapatite. *CAMEO: Conservation and Art Materials Encyclopedia Online* [online]. [cit. 2020-06-26]. Dostupné z: http://cameo.mfa.org/wiki/Calcium_hydroxyapatite

[41] KANG, Suk-Joong, L. *Sintering: Densification, Grain Growth and Microstructure*. Butterworth-Heinemann, 2004. ISBN 978-0750663854.

[42] JEMELKA, Marek. Studium vývoje mikrostruktury pokročilých keramických materiálů ve druhé fázi slinování [online]. Brno, 2019 [cit. 2019-05-22]. Dostupné z: https://www.vutbr.cz/studenti/zavprace/detail/116095. Diplomová práce. Vysoké učení technické v Brně, Fakulta strojního inženýrství, Ústav materiálových věd a inženýrství. Vedoucí práce Karel Maca.

[43] Wettability in Oil and Gas Reservoirs. *Exploration and Production Geology* [online]. [cit. 2020-06-26]. Dostupné z: http://www.epgeology.com/reservoir-engineering-f10/wettability-oil-and-gas-reservoirs-t5978.html

[44] LAW, Kock-Yee a Hong ZHAO. *Surface wetting: Characterization, Contact Angle, and Fundamentals*. Springer International Publishing, 2016. ISBN 978-3-319-25212-4.

[45] GOLDSTEIN, A.H. and Schade, G.W. (2000) *Quantifying biogenic and anthropogenic contributions to acetone mixing ratios in a rural environment.* Atmospheric Environment, 34: 4997‑5006.

[46] JACOB, D.J., Field, B.D., Jin, E.M., et al. (2002) *Atmospheric budget of acetone.* Journal of Geophysical Research – Atmospheres, 107(D10): 4100.

[47] JACOB, D.J., Field, B.D., Li, Q.B., et al. (2005) *Global budget of methanol:Constraints fromatmospheric observations*. Journal of Geophysical Research – Atmospheres, 110: D08303

[48] SINGH, H.B., Salas, L.J., Chatfield, R.B., et al. (2004) *Analysis of the atmospheric distribution, sources, and sinks of oxygenated volatile organic chemicals based on measurements over the Pacific during TRACE-P*. Journal of Geophysical Research – Atmospheres, 109: D15S07.

9 LIST OF TABLES

Tables

10 LIST OF FIGURES

Figures

11 LIST OF SYMBOLS

$\mathcal{A}$	Hamaker constant	J
A_{LJ}	Lennard-Jones potential	Jm^6
B	bulk density	$g \cdot cm^{-3}$
B_{LJ}	Lennard-Jones potential	Jm^{12}
E	energy of crystal	J
f	acting force	N
f_f	frictional force	N
$F_d(t)$	driving force of spreading	$N \cdot m^{-1}$
k	parameter determined from experimental data	-
l	length	m
m	mass of the unit cell	g
m_d	Mass of a dried sample	g
m_{dry}	Mass of a dry sample	g
m_w	Mass of a wet sample	g
$m_{unitcell}$	weight of the unit cell	g
r	distance	m
R	parameter of length	m
T_m	melting temperature	°C
T_{H_2O}	temperature of deionized water	°C
V_{bulk}	volume of the crystalline phases and the porosity	cm^{-3}
V_O	volume of open porosity	%
V_P	volume of pores	$g \cdot cm^{-3}$

V_S	volume of the solid phase	$g \cdot cm^{-3}$
$V_{unitcell}$	volume of the unit cell	cm^3
W_{sl}	work of adhesion between solid and liquid phase	$N \cdot m^{-1}$
X_M	electronegativity of cation	-
X_X	electronegativity of anion	-
γ_{lg}	interfacial tension between liquid phase and gaseous phase	$N \cdot m^{-1}$
γ_{sg}	interfacial tension between solid phase and gaseous phase	$N \cdot m^{-1}$
γ_{sl}	interfacial tension between solid phase and liquid phase	$N \cdot m^{-1}$
γ_{xy}	interfacial tensions between phases	$N \cdot m^{-1}$
θ	contact angle	°
$\theta(t)$	contact angle evolution in time	°
θ_{max}	advancing contact angle	°
θ_{min}	receding contact angle	°
ρ	crystallographic density	$g \cdot cm^{-3}$
ρ_{H_2O}	density of deionized water	$g \cdot cm^{-3}$
ρ_{rel1}	relative density	%
ρ_{theor}	theoretical density	$g \cdot cm^{-3}$
ρ_1, ρ_2	number of atoms per unit volume in two solids	m^{-3}
σ	Surface tension	$N \cdot m^{-1}$

12 LIST OF ABBREVIATIONS

ACA	Advancing contact angle	-
AES	Auger Electron Spectroscopy	-
AL15	Al_2O_3 sintered at 1500°C	-
AL16	Al_2O_3 sintered at 1600°C	-
ASTM	International standards – American Society for Testing and Materials	-
Confidence Interval -low	Lower boundary of confidence interval	°
Confidence Interva -up	Upper boundary of confidence interval	°
HA	hydroxyapatite	-
HA11	Hydroxyapatite sintered at 1100°C	-
LEIS	Low-Energy Ion Scattering	-
RBS	Detergent concentrate – cleaning agent	-
RCA	Receding contact angle	-
SSS	Solid-state sintering	-
TI11	TiO_2 sintered at 1100°C	-
TOF-SIMS	Time-of-flight Secondary Ion Mass Spectroscopy	-
UVO	Ultraviolet-Ozone surface treatment	-
VOC	Volatile organic compounds	-

WCA	Water contact angle	°
XPS	X-ray photoelectron spectroscopy	-
ZN11	ZnO sintered at 1100°C	-
ZR13	ZrO_2 sintered at 1300°C	-
ZR14	ZrO_2 sintered at 1400°C	-
ZR15	ZrO_2 sintered at 1500°C	-
ZR16	ZrO_2 sintered at 1600°C	-
3Y-TZP	3 mol% yttria stabilized tetragonal zirconia	-